This is the peer-reviewed, final accepted version for American Mineralogist, published by the Mineralogical Society of America.
The published version is subject to change. Cite as Authors (Year) Title. American Mineralogist, in press.
DOI: https://doi.org/10.2138/am-2022-8900. http://www.minsocam.org/

REVISION 3

Influence of anisotropy on the electrical conductivity of apatite at high temperatures and high pressures

Ziming Hu[1,2], Lidong Dai[1*], Haiying Hu[1*], Wenqing Sun[1], Mengqi Wang[1,2], Chenxin Jing[1,2], Chuanyu Yin[1,2], Song Luo[1,2], and Jinhua Lai[1,2]

[1]Key Laboratory of High-Temperature and High-Pressure Study of the Earth′s Interior, Institute of Geochemistry, Chinese Academy of Sciences, Guiyang, 550081, China

[2]University of Chinese Academy of Sciences, Beijing, 100049, China

To be submitted to ***American Mineralogist***

December 22th, 2022

Revised on June 27th, 2023

*Authors to whom correspondence should be addressed: dailidong@vip.gyig.ac.cn and huhaiying@vip.gyig.ac.cn

Always consult and cite the final, published document. See http:/www.minsocam.org or GeoscienceWorld

This is the peer-reviewed, final accepted version for American Mineralogist, published by the Mineralogical Society of America.
The published version is subject to change. Cite as Authors (Year) Title. American Mineralogist, in press.
DOI: https://doi.org/10.2138/am-2022-8900. http://www.minsocam.org/

Abstract

The *in-situ* electrical conductivity of apatite single crystals along three main crystalline directions were measured using the YJ–3000t multi–anvil apparatus and a combined system consisting of the impedance/gain–phase analyzer (Solartron 1260) and dielectric interface (Solartron 1296) at conditions of 973–1373 K and 1.0–3.0 GPa. Experimental results indicate that the relationship between the electrical conductivity of sample and temperature conforms to the Arrhenius relation. At 2.0 GPa, the electrical conductivity of apatite with relatively high activation enthalpies of 1.92–2.24 eV shows a significant anisotropy with the extremely high anisotropic degree (τ = ~8–16) value. For a given [001] crystallographic orientation, the electrical conductivity of apatite slightly decreases with increasing pressure, and its corresponding activation energy and activation volume of charge carriers are calculated as 2.05 ± 0.06 eV and 9.31 ± 0.98 cm^3/mole, respectively. All of these observed anomalously high activation enthalpy and positive activation volume values suggest that the main conduction mechanism of sample is related to the monovalent fluorine anion at high temperature and high pressure. Furthermore, three representative petrological average schemes including the parallel, Hashin–Shtrikman upper bound and average models were selected to establish the functional relation for the electrical conductivity of the phlogopite–apatite–peridotite rock system along with the volume percentages of apatite ranging from 1% to 10% at conditions of 973–1373 K and 2.0 GPa. For a typical Hashin–Shtrikman upper bound model, the electrical

Always consult and cite the final, published document. See http:/www.minsocam.org or GeoscienceWorld

This is the peer-reviewed, final accepted version for American Mineralogist, published by the Mineralogical Society of America.
The published version is subject to change. Cite as Authors (Year) Title. American Mineralogist, in press.
DOI: https://doi.org/10.2138/am-2022-8900. http://www.minsocam.org/

conductivity–depth profile for peridotite containing the 10% volume percentage of apatite was successfully constructed in conjunction with our acquired anisotropic electrical conductivity results and available temperature gradient data (11.6 K/km and 27.6 K/km) at depths of 20–90 km. Although the presence of apatite in peridotite cannot explain the high conductivity anomalies in western Junggar of Xinjiang autonomous region, it can provide a reasonable constraint on those of representative apatite–rich areas.

Keywords: Apatite; electrical conductivity; anisotropy; fluorine conduction; high pressure

Always consult and cite the final, published document. See http:/www.minsocam.org or GeoscienceWorld

This is the peer-reviewed, final accepted version for American Mineralogist, published by the Mineralogical Society of America.
The published version is subject to change. Cite as Authors (Year) Title. American Mineralogist, in press.
DOI: https://doi.org/10.2138/am-2022-8900. http://www.minsocam.org/

Introduction

Previously available field geophysical magnetotelluric (MT) results revealed that there existed phenomena of widespread high conductivity anomalies and highly electrical conductivity anisotropy in many areas of the lithosphere and asthenosphere (Hamilton et al. 2006; Naif et al. 2013; Selway 2014, 2015, 2019; Selway and O'Donnell 2019; Selway et al. 2019; Förster and Selway 2021; Özaydın and Selway 2022). For a typical geotectonic unit in western Junggar of Xinjiang autonomous region, the remnants of subducted oceanic slab with the anomalous high conductivity range of ~10^{-2}–1 S/m have been reported on the basis of recent MT data (Xu et al. 2016, 2020; Zhang et al. 2017; Liu et al. 2019a). *In-situ* electrical conductivity measurements of relevant minerals and rocks under high–temperature and high–pressure conditions can be applied to reasonably interpret the observed MT results. As pointed out by Xu et al. (2020), the high conductivity anomalies in the western Junggar of Xinjiang autonomous region can be caused by the presence of volatile–bearing metasomatic minerals (VMMs), such as apatite, phlogopite, lawsonite and amphibole in the residual oceanic plate.

Generally, the volatile–bearing metasomatic minerals are the ordinary constituent materials to mantle magma, which also exist as a disseminated type in the mantle peridotite. As a research hotpoint, the electrical properties of VMMs at high temperature and high pressure have attracted great attention in the recently several years (Manthilake et al. 2015, 2016, 2021a, b; Li et al. 2016, 2017; Hu et al. 2018; Liu

Always consult and cite the final, published document. See http:/www.minsocam.org or GeoscienceWorld

This is the peer-reviewed, final accepted version for American Mineralogist, published by the Mineralogical Society of America.
The published version is subject to change. Cite as Authors (Year) Title. American Mineralogist, in press.
DOI: https://doi.org/10.2138/am-2022-8900. http://www.minsocam.org/

et al. 2019b; Ye et al. 2022). For a representative water–bearing and fluorine–bearing silicate mineral, Li et al. (2016) investigated the electrical conductivity of phlogopite single crystals along three main crystalline directions at temperature range of 473–1173 K and pressure of 1.0 GPa with an end–loaded piston cylinder press. They observed anomalously high conductivity and significant electrical conductivity anisotropy of phlogopite, which can account for the regional high conductivity anomalies in the continental upper mantle. As far as a typically hydrous silicate mineral in oceanic subduction slab, Manthilake et al. (2015) performed the electrical conductivity measurements of lawsonite at 298–1320 K and 7.0 GPa by virtue of the Kawai–1500t multi–anvil high–pressure apparatus. They found that the highly conductive fluid from the dehydration of lawsonite can lead to those of regional high conductivity anomalies of northern Chilean subduction zone, central Chilean subduction zone and northeastern Japan within the depth range of 150–275 km. For a predominant rock–forming mineral in the mid–lower Earth crust and subduction zone, the electrical conductivity of iron–bearing amphibole single crystals was systematically investigated by Hu et al. (2018) at temperatures of 523–1173 K and pressures of 0.5–2.0 GPa using the YJ–3000t multi–anvil high–pressure apparatus. All of these acquired experimental results from Hu et al. (2018) indicated that the electrical conductivity of amphibole was highly sensitive to temperature, pressure and oxidation–dehydrogenation process. Due to the occurrence of oxidation–dehydrogenation, the enhanced electrical conductivity of amphibole can reasonably

Always consult and cite the final, published document. See http:/www.minsocam.org or GeoscienceWorld

This is the peer-reviewed, final accepted version for American Mineralogist, published by the Mineralogical Society of America.
The published version is subject to change. Cite as Authors (Year) Title. American Mineralogist, in press.
DOI: https://doi.org/10.2138/am-2022-8900. http://www.minsocam.org/

84 explain the high conductivity anomalies in the stable continental lowermost mid–crust
85 and slab–mantle wedge interfaces. However, as a crucial volatile–bearing
86 metasomatic mineral, so far, there is no reported data about the electrical conductivity
87 of apatite under high temperature and high pressure conditions.

88 Apatite is a type of important calcium–bearing and volatile–bearing phosphate
89 mineral, which widely exists as an accessory mineral in a large number of igneous,
90 sedimentary and metamorphic rocks. As the major source of phosphorous ore, the
91 high–pressure physiochemical investigations on apatite are essential to explore the
92 geological cycle of global phosphorus element in the deep Earth′s interior. Most of
93 reported data about the high–pressure compressibility, thermal expansion coefficient
94 and *P–T* phase diagram on apatite were obtained by *in–situ* synchrotron X–ray
95 diffraction and Raman spectroscopy measurements (Murayama et al. 1986; Brunet et
96 al. 1999; Comodi et al. 2001a, b; Matsukage et al. 2004; Konzett and Frost 2009). It is
97 well known that apatite is a representative hexagonal mineral with the relatively low–
98 symmetric crystalline structure. All of these data including the high–pressure thermal
99 expansion coefficient and compressibility reported by Brunet et al. (1999) and
100 Comodi et al. (2001a), as well as the element diffusivity reported by Brenan (1994)
101 and Li et al. (2020), have indicated the significant effect of crystallographic orientation
102 on the physiochemical properties of the low–symmetric apatite single crystal.
103 Electrical conductivity is also highly sensitive to the crystallographic orientation for
104 some typical low–symmetric silicate minerals (e.g., olivine, pyroxene, phlogopite, K–

Always consult and cite the final, published document. See http:/www.minsocam.org or GeoscienceWorld

This is the peer-reviewed, final accepted version for American Mineralogist, published by the Mineralogical Society of America.
The published version is subject to change. Cite as Authors (Year) Title. American Mineralogist, in press.
DOI: https://doi.org/10.2138/am-2022-8900. http://www.minsocam.org/

feldspar, etc.), which widely outcrop in the regions of mid–lower Earth crust and upper mantle (Huebner and Voigt 1988; Yang 2012; Dai and Karato 2014a; Li et al. 2016; Dai et al. 2018a, 2022). Nevertheless, until now, the effect of high–pressure crystallographic orientation on the electrical conductivity of apatite remains unclear.

In the present study, the *in-situ* electrical conductivity of apatite single crystals along three main [001], [100] and [010] crystalline directions were investigated at temperatures of 973–1373 K and pressures of 1.0–3.0 GPa. The influences of temperature, pressure and crystallographic orientation on the electrical conductivity were explored in detail. Furthermore, the functional dependence relation for the volume percentages of apatite on the electrical conductivity of the phlogopite–apatite–peridotite rock system was successfully constructed. Finally, the electrical conductivity–depth profile for peridotite containing the 10% volume percentage of apatite was established, and profoundly discussed its geophysical implications.

Experimental procedures

Sample preparation

In this study, a natural gem–grade apatite single crystal with the perfect hexagonal structure and its dimension of ~20×15×15 mm^3 was collected from Lianyungang city, Jiangsu province, China. Apatite single crystal was fresh with the transparent yellow surface color, vitreous luster and no evidences of twinning, exsolution or alteration. The chemical composition of sample was checked by the

Always consult and cite the final, published document. See http:/www.minsocam.org or GeoscienceWorld

This is the peer-reviewed, final accepted version for American Mineralogist, published by the Mineralogical Society of America.
The published version is subject to change. Cite as Authors (Year) Title. American Mineralogist, in press.
DOI: https://doi.org/10.2138/am-2022-8900. http://www.minsocam.org/

JEOL JXA–8230 electron microprobe analyzer (EPMA) operated at the State Key Laboratory of Ore-Deposit Geochemistry, Institute of Geochemistry, Chinese Academy of Sciences (CAS), as shown in Table 1. It is obvious that our sample belongs to a representative calcium–bearing, volatile–bearing (fluorine–containing and chloride–containing) and nominally anhydrous phosphate fluorapatite with the relatively high fluorine content up to 4.33 ± 0.02 wt.%. In this study, the hexagonal apatite single crystal along the long crystallographic orientation is nominated as the [001] crystalline direction, and other two mutually perpendicular crystallographic orientations are nominated as the [100] and [010] crystalline directions. Accordingly, the representative optical microscopic observation and its corresponding crystalline structure of apatite are also displayed in Figure 1. Then, the crystal was cut and polished to circular columns (Spec: 6.0 mm of diameter and 4.0 mm of height) along three main [001], [100] and [010] crystalline directions. After that, the cylindrical samples were rinsed using the acetone, ethanol and de–ionized water in an ultrasonic cleaner. Finally, the samples were kept in a muffle furnace at 423 K for 10 hrs to eliminate the absorbed water for subsequent electrical conductivity measurements.

Sample characterization

The water content of samples before and after the electrical conductivity measurements was investigated by using a Vertex–70V vacuum Fourier transform infrared (FT–IR) spectroscopy analyzer. Samples were cut and doubly polished to a

Always consult and cite the final, published document. See http:/www.minsocam.org or GeoscienceWorld

This is the peer-reviewed, final accepted version for American Mineralogist, published by the Mineralogical Society of America.
The published version is subject to change. Cite as Authors (Year) Title. American Mineralogist, in press.
DOI: https://doi.org/10.2138/am-2022-8900. http://www.minsocam.org/

thickness of less than 150 μm using the diamond blade for subsequent FT–IR analysis. The FT–IR spectra were collected according to the total absorbance of OH groups between wavenumbers of 3000–4000 cm^{-1} with the accumulation of 512 scans for each sample. As shown in Figure 2, the representative FT–IR spectra for initial and recovered samples exhibit a sharp absorbance peak at the characteristic wavenumber position of ~3560 cm^{-1}, which is in good agreement with previously reported FT–IR results of apatite single crystal for Wang et al. (2011). According to the Beer–Lambert law, the water content (C_w) in apatite single crystals can be calculated by the following formula,

$$C_w = \omega A / \varepsilon \rho d \quad (1)$$

where A is the total integrated absorbance (1/cm), ω represents the molar mass of H_2O (18.02 g/mole), ρ is the density of sample (3.20 g/cm^3), d is the thickness of sample (cm), and ε is the molar absorptivity of sample [2.31×10^4 $L/(mole\cdot cm^2)$] to be reported by Wang et al. (2011). The water contents of starting and recovered apatite single crystals were calculated as 176.69 ppm wt and 134.87 ppm wt, respectively, which suggests no clear water loss during the process of electrical conductivity measurements.

High–pressure cell and complex impedance measurements

Complex impedance measurements of samples were conducted using the YJ–3000t multi–anvil apparatus and a combined system consisting of the

Always consult and cite the final, published document. See http:/www.minsocam.org or GeoscienceWorld

This is the peer-reviewed, final accepted version for American Mineralogist, published by the Mineralogical Society of America.
The published version is subject to change. Cite as Authors (Year) Title. American Mineralogist, in press.
DOI: https://doi.org/10.2138/am-2022-8900. http://www.minsocam.org/

impedance/gain–phase analyzer (Solartron 1260) and dielectric interface (Solartron 1296). Experimental principles and measurement procedures were described by Dai et al. (2012) and Hu et al. (2017) in detail. Figure 3 displays the cross–section diagram of the sample assemblage for high–pressure impedance spectroscopy measurements. Pressure–transmitting medium of cubic pyrophyllite with a dimension of 32.5×32.5×32.5 mm^3 was baked at 1073 K for 8 hrs to avoid the influence of dehydration on the electrical conductivity results. Some components of the experimental assemblage (alumina sleeve, magnesia sleeves and ceramic tube) were kept at 423 K in a muffle furnace for 10 hrs to remove the absorbed water. The heater was consisted of three–layer stainless steel sheets with a total thickness of 0.5 mm. Alumina and magnesia sleeves were employed to provide an excellent insulation environment during the process of high–pressure electrical conductivity measurements. The nickel foil with its corresponding thickness of 25 μm connected to the ground was installed between alumina and magnesia sleeves, which can efficiently prevent the current leakage of high–pressure experimental assemblage. A cylindrical sample (Spec: 6.0 mm × 4.0 mm) was laid in the center of electrical conductivity assemblage. Two symmetric nickel slices with each thickness of 0.5 mm at both ends of sample were adopted as electrodes, which also can be adopted to control and adjust the oxygen fugacity in the sample chamber. The experimental temperatures were monitored by a $Ni_{90}Cr_{10}$–$Ni_{97}Al_3$ thermocouple. Measurement uncertainties from the experimental temperature and pressure were ±5 K and ±0.1 GPa, respectively.

Always consult and cite the final, published document. See http:/www.minsocam.org or GeoscienceWorld

This is the peer-reviewed, final accepted version for American Mineralogist, published by the Mineralogical Society of America.
The published version is subject to change. Cite as Authors (Year) Title. American Mineralogist, in press.
DOI: https://doi.org/10.2138/am-2022-8900. http://www.minsocam.org/

186 During the experiment, pressure was raised to the designated value at a rate of 1.0
187 GPa/h. Under constant pressure condition, temperature was gradually increased to the
188 desired value at an interval of 50 K. Subsequently, the complex impedance spectra of
189 apatite were continuously collected within the temperature range from 973 K to 1373
190 K. The fixed signal voltage of 1.0 V and frequency range of 10^{-1}–10^{6} Hz were applied,
191 respectively. To obtain reproducible data, the complex impedance spectra of the
192 samples were measured in two subsequent heating–cooling cycles. In order to check
193 the insulation property of the assemblage background, the electrical conductivity of a
194 cylindrical magnesium oxide with the diameter of 6.0 mm and height of 4.0 mm was
195 investigated at a wider temperature range from 1073 K to 1523 K and 2.0 GPa. At a
196 relatively low temperature of 1073 K, the electrical conductivity of magnesium oxide
197 is approximately 3.2 times lower than that of [010] crystallographic orientation, and
198 approximately 29.4 times lower than that of [001] crystallographic orientation, as
199 detailedly displayed in Figure 7. With the rise of temperature, the discrepancy of the
200 electrical conductivity in apatite and magnesium oxide increases, and thus, the
201 insulation property of assemblage background becomes better. At a relatively high
202 temperature of 1373 K, the electrical conductivity of magnesium oxide is
203 approximately 32.3 times lower than that of [010] crystallographic orientation, and
204 more than 500 times lower than that of [001] crystallographic orientation. As a typical
205 insulation material of magnesium oxide, it can provide an extremely good insulation,
206 especially among the high–temperature electrical conductivity of apatite.

Always consult and cite the final, published document. See http:/www.minsocam.org or GeoscienceWorld

This is the peer-reviewed, final accepted version for American Mineralogist, published by the Mineralogical Society of America.
The published version is subject to change. Cite as Authors (Year) Title. American Mineralogist, in press.
DOI: https://doi.org/10.2138/am-2022-8900. http://www.minsocam.org/

Results

In the present experiments, the electrical conductivity of apatite single crystals along three main [001], [100] and [010] crystalline directions was measured in the temperature range of 973–1373 K and pressure of 2.0 GPa. To deeply explore the influence of pressure on the electrical conductivity, measurements of samples along a fixed [001] crystallographic orientation were also carried out within the pressure range from 1.0 GPa to 3.0 GPa.

Representative complex impedance spectra for apatite single crystal of the [010] crystallographic orientation at conditions of 973–1373 K and 2.0 GPa are shown in Figure 4. All of the complex impedance spectra at each corresponding temperature point are composed of an almost ideal semicircular arc within the high–frequency range and a tiny tail at low frequency. According to the theory of *AC* complex electrochemical impedance spectroscopy (Huebner and Dillenburg 1995; Yang and McCammon 2012; Saltas et al. 2013, 2020; Sivakumar et al. 2018, 2021, 2022; Dai and Karato 2020), our acquired semicircular arc and additional tiny tail stand for the electrical transport process of grain interior and polarization process at the sample–electrode interface, respectively. Therefore, an equivalent circuit composed of the series connection of parallel R_S–CPE_S and parallel R_E–CPE_E was employed to fit the impedance semicircular arc and determine the electrical resistance of apatite single crystal, where the symbols of R_S and CPE_S represent the electrical resistance and constant phase element for the sample, respectively; R_E and CPE_E represent the

Always consult and cite the final, published document. See http:/www.minsocam.org or GeoscienceWorld

This is the peer-reviewed, final accepted version for American Mineralogist, published by the Mineralogical Society of America.
The published version is subject to change. Cite as Authors (Year) Title. American Mineralogist, in press.
DOI: https://doi.org/10.2138/am-2022-8900. http://www.minsocam.org/

228 electrical resistance and constant phase element for the polarization process at the
229 sample–electrode interface, respectively. Then, the electrical conductivity of the
230 sample (σ) was calculated as follows,

231 $$\sigma = L/RS \quad (2)$$

232 where L, S and R are the length of sample (m), the cross–section area of electrode (m^2),
233 and the electrical resistance of sample (Ω), respectively.

234 Figure 5 shows the logarithmic electrical conductivity of apatite in the [001]
235 crystallographic orientation against the reciprocal temperature for two continuous
236 heating–cooling cycles ranging from 973 K to 1373 K and 3.0 GPa. It is clear that the
237 electrical conductivity in the first heating cycle is higher than those in the subsequent
238 cooling and second heating–cooling cycles at a relatively low temperature range from
239 973 K to 1173 K. In the following first cooling and second heating–cooling cycles, the
240 electrical conductivity values show a good reproducibility over the whole measured
241 temperature range, which indicates that a completely stable and equivalent state is
242 reached in the sample chamber during the process of electrical conductivity
243 measurement. The reproducible data attained from the first cooling and subsequent
244 second heating–cooling cycles are used to fit the electrical conductivity results. The
245 relationship between the electrical conductivity of apatite and temperature can be
246 expressed by the Arrhenius relation,

247 $$\sigma = \sigma_0 \exp(-\Delta H/kT) \quad (3)$$

248 where σ_0, k and T are the pre–exponential factor (S/m), the Boltzmann constant (eV/K)

Always consult and cite the final, published document. See http:/www.minsocam.org or GeoscienceWorld

This is the peer-reviewed, final accepted version for American Mineralogist, published by the Mineralogical Society of America.
The published version is subject to change. Cite as Authors (Year) Title. American Mineralogist, in press.
DOI: https://doi.org/10.2138/am-2022-8900. http://www.minsocam.org/

and the absolute temperature (K), respectively. ΔH is the activation enthalpy (eV). The dependence relation of activation enthalpy on the pressure can be described as,

$$\Delta H = \Delta U + P\Delta V \quad (4)$$

where ΔU and ΔV are the activation energy (eV) and activation volume (cm^3/mole), respectively.

Figure 6 displays the influence of pressure on the electrical conductivity of apatite along the [001] crystallographic orientation at conditions of 973–1373 K and 1.0–3.0 GPa. The detailed electrical conductivity of apatite single crystals along three main [001], [100] and [010] crystalline directions at 973–1373 K and 2.0 GPa are illustrated in Figure 7. In addition, the background electrical conductivity of magnesium oxide is also included in Figure 7 over a wider temperature range from 1073 K to 1523 K at 2.0 GPa. All the fitting parameters for the electrical conductivity of apatite single crystals are detailedly listed in Table 2.

Discussions

Effect of pressure on electrical conductivity

For a fixed [001] crystallographic orientation, the pressure–dependent electrical conductivity of apatite is clearly displayed in Figure 6. It is clear that the electrical conductivity of the sample decreases by approximately 2.5 times at a certain temperature point as the pressure increases from 1.0 GPa to 3.0 GPa. Whereas, the magnitude of pre–exponential factor rises from 8.91×10^5 S/m to 2.09×10^6 S/m, and

Always consult and cite the final, published document. See http:/www.minsocam.org or GeoscienceWorld

This is the peer-reviewed, final accepted version for American Mineralogist, published by the Mineralogical Society of America.
The published version is subject to change. Cite as Authors (Year) Title. American Mineralogist, in press.
DOI: https://doi.org/10.2138/am-2022-8900. http://www.minsocam.org/

the activation enthalpy value increases from 2.14 eV to 2.33 eV, respectively. With the rise of pressure, the crystalline framework of apatite is gradually compressed, which leads to a narrower pathway of charge carrier, and thus, the relatively high energy is required for charge carrier to cross the energy barrier. This is reflected in the reduced electrical conductivity and increased activation enthalpy of samples at higher pressure conditions. The negative influence of pressure on the electrical conductivity was also observed for some silicate minerals, such as olivine, anorthite, plagioclase, kaolinite, etc. (Xu et al. 2000; Dai and Karato 2014b; Hu et al. 2015, 2022a; Hong et al. 2022). According to equation (4) and Table 2, the activation energy and the activation volume of charge carriers are calculated as 2.05 ± 0.06 eV and 9.31 ± 0.98 cm^3/mole, respectively. In light of the available pressure–dependent electrical conductivity, we can also extrapolate the relationship between the electrical conductivity of apatite and temperature at atmospheric pressure, as illustrated in Figure 6.

Effect of crystallographic orientation on electrical conductivity

For a fixed pressure of 2.0 GPa, the influence of crystallographic orientation on the electrical conductivity of apatite single crystal at temperatures of 973–1373 K is detailedly depicted in Figure 7. The electrical conductivity of the background of magnesium oxide is included at a wider temperature range from 1073 K to 1523 K and 2.0 GPa. It is clear that the electrical conductivity of sample increases along an order of [010], [100] and [001] crystallographic orientations, and their corresponding

Always consult and cite the final, published document. See http:/www.minsocam.org or GeoscienceWorld

This is the peer-reviewed, final accepted version for American Mineralogist, published by the Mineralogical Society of America.
The published version is subject to change. Cite as Authors (Year) Title. American Mineralogist, in press.
DOI: https://doi.org/10.2138/am-2022-8900. http://www.minsocam.org/

activation enthalpies are determined to be 1.92–2.24 eV. Figure 8 displays the degree of electrical conductivity anisotropy ($\tau = \sigma_{Max}/\sigma_{Min}$) for apatite single crystals and apatite polycrystalline aggregates as a function of temperature from 900 K to 1700 K. Our present obtained electrical conductivity results for olivine containing the 10% volume percentage of apatite, and previously available results for the electrical conductivity of hydrous olivine single crystals reported by Dai and Karato (2014a), as well as the electrical conductivity of the field geophysical observations in asthenosphere from Evans et al. (2005) and Naif et al. (2013) are also clearly illustrated in Figure 8. The degree of electrical conductivity anisotropy ($\tau = \sigma_{Max}/\sigma_{Min}$) for olivine containing the 10% volume percentage of apatite is calculated using our present anisotropic electrical conductivity data and the Hashin–Shtrikman upper bound model, which is detailedly presented as,

$$\tau_{HS+}=\tau_{Ol} + \frac{f_{Ap}}{(\tau_{Ap}-\tau_{Ol})^{-1} + f_{Ol}(3\tau_{Ol})^{-1}} \quad (5)$$

where τ_{Apa} and τ_{Ol} are the degrees of electrical conductivity anisotropy of apatite single crystal and olivine single crystal, respectively; f_{Apa} and f_{Ol} are the volume percentages of apatite single crystal and olivine single crystal, respectively.

As detailedly described in Figure 8, the degree of electrical conductivity anisotropy for apatite single crystal displays an available positive linear dependence relation with temperature at 2.0 GPa. With increasing temperature from 700 K to 1700 K, the degree of electrical conductivity anisotropy for apatite single crystal increases from ~7 to ~23. Accordingly, the degree of electrical conductivity anisotropy for

Always consult and cite the final, published document. See http:/www.minsocam.org or GeoscienceWorld

This is the peer-reviewed, final accepted version for American Mineralogist, published by the Mineralogical Society of America.
The published version is subject to change. Cite as Authors (Year) Title. American Mineralogist, in press.
DOI: https://doi.org/10.2138/am-2022-8900. http://www.minsocam.org/

apatite polycrystalline aggregates is also enhanced from ~0.50 to ~1.65, which reveals the existence of more significant electrical conductivity anisotropy for apatite single crystal under condition of the higher temperature of deeper Earth′s interior. On the other hand, the degree of electrical conductivity anisotropy for apatite becomes higher than that of hydrous olivine at temperatures below ~1320 K, and lower than that of hydrous olivine in the temperature range of 1320–1700 K. The degrees of electrical conductivity anisotropy for olivine containing the 10% volume percentage of apatite and hydrous olivine single crystal exhibit similar tendency with the variation of temperature. These results can be transformed into the degree of electrical conductivity anisotropy for polycrystalline aggregates using the numerical research on olivine single crystals to be reported by Simpson and Tommasi (2005). As pointed out by McKenzie and Bickle (1988), the temperature in the region of mantle asthenosphere falls within the range of 1550–1650 K. Previous geophysical observations have indicated that the degree of electrical conductivity anisotropy in the asthenosphere can be up to a factor of ~2–3 higher along the flow direction on the horizontal plane (Evans et al. 2005; Naif et al. 2013). For the representative peridotite–dominated asthenospheric temperature condition, it is clear that the obtained degree of electrical conductivity anisotropy value for apatite is much lower than those of field geophysical observations. The degree of conductivity anisotropy observed in the asthenosphere is dominated by the anisotropic electrical conductivity of hydrous olivine.

Always consult and cite the final, published document. See http:/www.minsocam.org or GeoscienceWorld

This is the peer-reviewed, final accepted version for American Mineralogist, published by the Mineralogical Society of America.
The published version is subject to change. Cite as Authors (Year) Title. American Mineralogist, in press.
DOI: https://doi.org/10.2138/am-2022-8900. http://www.minsocam.org/

The acquired highly electrical conductivity anisotropy of apatite may be resulted in by the anisotropic mobility of charge carrier, which is possibly correlated with its low–symmetric crystalline structure (Fig. 1b). In combination with the measured anisotropic electrical conductivity results, three spatial averaging schemes were employed to extrapolate the isotropic electrical conductivity of randomly oriented apatite polycrystalline aggregates at high temperature and high pressure. In the present study, three representative averaging schemes on the electrical conductivity of apatite single crystals including series (σ_S), parallel (σ_P), and average (σ_A) models are presented as follows,

$$\sigma_S = \frac{3}{1/\sigma_{[001]} + 1/\sigma_{[100]} + 1/\sigma_{[010]}} \quad (6)$$

$$\sigma_P = \frac{\sigma_{[001]} + \sigma_{[100]} + \sigma_{[010]}}{3} \quad (7)$$

$$\sigma_A = \frac{\sigma_S + \sigma_P + \sqrt{(\sigma_S + \sigma_P)^2 + 32\sigma_S\sigma_P}}{8} \quad (8)$$

By virtue of three above–mentioned isotropic average schemes, the acquired anisotropic electrical conductivity results on apatite along the [010], [100] and [001] crystalline directions were transformed into isotropic conductivity values for randomly oriented apatite polycrystalline aggregates. As pointed out by Dai and Karato (2014a) and Hu et al. (2022b), the electrical conductivity results from the series and parallel models represent the lower and upper boundary values in the isotropic average schemes of polycrystalline aggregates, respectively.

Comparisons with other VMMs

Always consult and cite the final, published document. See http:/www.minsocam.org or GeoscienceWorld

This is the peer-reviewed, final accepted version for American Mineralogist, published by the Mineralogical Society of America.
The published version is subject to change. Cite as Authors (Year) Title. American Mineralogist, in press.
DOI: https://doi.org/10.2138/am-2022-8900. http://www.minsocam.org/

For the representative geotectonic unit in western Junggar of Xinjiang autonomous region, Xu et al. (2020) proposed that there existed four interconnected VMMs of apatite, phlogopite, lawsonite and amphibole, which can be employed to explain the anomalously high conductivity from the field geophysical MT results. Therefore, investigations on the electrical properties of VMMs at elevated temperature and pressure conditions are crucial in deeply exploring the origin of high conductivity anomalies in western Junggar of Xinjiang autonomous region. In this study, we systemically investigated the electrical conductivity of apatite along three main [001], [100] and [010] crystallographic orientations at conditions of 973–1373 K and 1.0–3.0 GPa. Thus, our absolutely new results for the anisotropic electrical conductivity of apatite single crystals were compared with the previously available data of other VMMs (i.e., phlogopite, lawsonite and amphibole), which is displayed in Figure 9. As a whole, the anisotropic electrical conductivity of apatite single crystals at 2.0 GPa are abnormally lower than those of three other representative VMMs for phlogopite from Li et al. (2016), lawsonite from Manthilake et al. (2015) and amphibole from Hu et al. (2018) at temperature range of 973–1373 K. As a hydrous and fluorine–bearing silicate mineral, Li et al. (2016) investigated the electrical conductivity of phlogopite single crystals along various crystalline directions at temperatures of 473–1173 K and pressure of 1.0 GPa. In comparison, the degree of electrical conductivity anisotropy in apatite (τ = ~8–16) is much higher than that of phlogopite (τ = ~4–12) at temperatures of 973–1373 K, which implies a stronger

Always consult and cite the final, published document. See http:/www.minsocam.org or GeoscienceWorld

This is the peer-reviewed, final accepted version for American Mineralogist, published by the Mineralogical Society of America.
The published version is subject to change. Cite as Authors (Year) Title. American Mineralogist, in press.
DOI: https://doi.org/10.2138/am-2022-8900. http://www.minsocam.org/

372 dependence relation of anisotropic conductivity in the apatite single crystal at high
373 temperature and high pressure. Meanwhile, the acquired activation enthalpies of 1.92–
374 2.24 eV for the anisotropic electrical conductivity of apatite are slightly higher than
375 those of phlogopite (1.37–2.08 eV). For a representative hydrous silicate mineral in
376 the oceanic subducted slab, Manthilake et al. (2015) performed the electrical
377 conductivity measurements of lawsonite at temperature range of 298–1320 K and 7.0
378 GPa. As reported by Manthilake et al. (2015), a sharp enhancement in electrical
379 conductivity was observed as the temperature exceeding 1258 K, which can be
380 ascribed to the dehydration of lawsonite. Their acquired activation enthalpies of 0.21–
381 0.98 eV on lawsonite are much lower than those of our present results for apatite. As
382 far as a predominant rock–forming mineral in the mid–lower Earth crust and
383 subduction zone, the electrical conductivity of iron–bearing amphibole single crystals
384 was measured by Hu et al. (2018) at conditions of 623–1173 K and 0.5–2.0 GPa.
385 During their experiment, the occurrence of oxidation–dehydrogenation reaction was
386 put forward at a temperature of ~843 K, which greatly enhanced the electrical
387 conductivity of amphibole. The dominant conduction mechanism of amphibole was
388 small polaron conduction with the relatively low activation enthalpies of 0.70–0.80 eV,
389 which are much lower than our acquired activation enthalpy results of apatite. In
390 summary, the electrical conductivity of apatite along different crystalline directions is
391 much lower than those of other representative VMMs (i.e., phlogopite, lawsonite and
392 amphibole) at temperature range of 973–1373 K. Likewise, our observed highly

Always consult and cite the final, published document. See http:/www.minsocam.org or GeoscienceWorld

This is the peer-reviewed, final accepted version for American Mineralogist, published by the Mineralogical Society of America.
The published version is subject to change. Cite as Authors (Year) Title. American Mineralogist, in press.
DOI: https://doi.org/10.2138/am-2022-8900. http://www.minsocam.org/

anisotropic electrical conductivity of apatite single crystals with relatively high activation enthalpies (1.92–2.24 eV) are possibly correlated with the unique hexagonal crystalline structure, as well as its mineralogical composition of the calcium–bearing and high–fluorine fluorapatite.

Conduction mechanism

The activation enthalpy for each conduction mechanism strongly depends on charge mobility, and the electrical transport mechanism can be distinguished by the variation in slope at given temperature range of the Arrhenius relation (Hu et al. 2015; Dai et al. 2016; Sun et al. 2017). For the newly attained data of apatite, only a linear relationship between the logarithmic electrical conductivity and reciprocal temperature is exhibited in the Arrhenius diagram, implying that only one dominant conduction mechanism, or several mechanisms with similar activation energy dominate the electrical transport of apatite within the limited temperature range of 973–1373 K and pressure range of 1.0–3.0 GPa.

In the present study, the relatively high activation enthalpies up to 1.92–2.24 eV were obtained for the electrical conductivity of apatite single crystals along three main [001], [100] and [010] crystalline directions at conditions of 973–1373 K and 2.0 GPa. Due to the existence of trace amount of water in our samples, the proton may be the dominant conduction mechanism for apatite at high temperature and high pressure. It is well known that the proton conduction is the most common defect species in many

Always consult and cite the final, published document. See http:/www.minsocam.org or GeoscienceWorld

This is the peer-reviewed, final accepted version for American Mineralogist, published by the Mineralogical Society of America.
The published version is subject to change. Cite as Authors (Year) Title. American Mineralogist, in press.
DOI: https://doi.org/10.2138/am-2022-8900. http://www.minsocam.org/

413 hydrous silicate minerals with a relatively low activation enthalpy of less than 1.0 eV,
414 such as hydrous amphibole, chlorite, glaucophane, etc. (Saltas et al. 2013; Manthilake
415 et al. 2016, 2021b). In view of the noticeable discrepancy in activation enthalpy
416 between proton conduction and our results, it cannot be the dominant conduction
417 mechanism for apatite. The small polaron conduction is considered to be an important
418 conduction mechanism for some anhydrous iron–bearing silicate minerals, such as
419 garnet, biotite and clinopyroxene (Dai et al. 2013; Saltas et al. 2020; Sun et al. 2020).
420 All of these obtained results have confirmed that small polaron conduction is
421 characterized by the activation enthalpy of <1.5 eV. Thus, the iron–free apatite single
422 crystals with relatively high activation enthalpies of 1.92–2.24 eV in this study can
423 rule out any contribution of small polaron. The observed values of high activation
424 enthalpy and positive activation volume for apatite conform to the characteristics of
425 ion conduction (Hu et al. 2015, Li et al. 2016, 2017). As shown in Table 1, calcium and
426 fluorine are two important constituent elements in our sample. According to the high–
427 temperature diffusion results reported by Cherniak (2010a), the diffusivity of calcium
428 cation is much lower than that of fluorine anion at the same temperature condition.
429 Therefore, the contribution of calcium cation to the electrical conduction of apatite
430 can be neglected. The most promising charge carrier in apatite is the fluorine anion,
431 which has a relatively small effective ionic radius (~1.17–1.25 Å) and high mobility at
432 elevated temperatures and pressures (Shannon 1976; Cherniak 2010b; Liu et al. 2019b).
433 In summary, on the basis of these obtained relatively high activation enthalpies,

Always consult and cite the final, published document. See http:/www.minsocam.org or GeoscienceWorld

This is the peer-reviewed, final accepted version for American Mineralogist, published by the Mineralogical Society of America.
The published version is subject to change. Cite as Authors (Year) Title. American Mineralogist, in press.
DOI: https://doi.org/10.2138/am-2022-8900. http://www.minsocam.org/

positive activation volume and appreciable fluorine content for the apatite sample, the monovalent fluorine anion was considered to be the main charge carrier for apatite under high–temperature and high–pressure conditions.

Implications

All of the previously available evidences from experimental petrology, isotopic geochemistry and field geophysics have revealed that apatite is a typical volatile–bearing mineral formed on the geotectonic environments of hydrothermal metasomatism (Roden et al. 1984; O'Reilly and Griffin 2000; Morishita et al. 2008; Marocchi et al. 2009; Efimov et al. 2012). As two correlated volatile–bearing accessory minerals, apatite and phlogopite are mutually accompanied, which are mainly enriched in the peridotite–predominated Earth mantle. As pointed out by Morishita et al. (2003, 2008), the field petrological observations and ion microprobe isotopic dating results have already confirmed that the highly metasomatized Finero phlogopite–peridotite massif was widely existed as an apatite-rich peridotite layer with its volume percentage of apatite up to 10% in the region of Italian Western Alps. For the representative electrical conductivity anomaly from the field geophysical magnetotelluric results in western Junggar of Xinjiang autonomous region, the high electrical conductivity with the corresponding magnitude of ~10^{-2}–1 S/m from Xu et al. (2020) is caused by the existence of four main volatile–bearing metasomatism minerals (i.e., apatite, phlogopite, lawsonite and amphibole).

Always consult and cite the final, published document. See http:/www.minsocam.org or GeoscienceWorld

This is the peer-reviewed, final accepted version for American Mineralogist, published by the Mineralogical Society of America.
The published version is subject to change. Cite as Authors (Year) Title. American Mineralogist, in press.
DOI: https://doi.org/10.2138/am-2022-8900. http://www.minsocam.org/

454 In order to explore the effect of the volume percentage of apatite on the electrical
455 conductivity of accessory mineralogical associations for the volatile–bearing
456 metasomatism minerals in the peridotite–predominated Earth mantle, we constructed
457 a phlogopite–apatite–peridotite rock system at high temperature and high pressure.
458 Previously available field petrological results indicated that the variation of
459 mineralogical volume fraction for two coexisting mineralogical associations of apatite
460 and phlogopite falls within the range of 1–10% in mantle peridotite (Griffin et al.
461 1984; O'Reilly 1987; O'Reilly and Griffin 2000; Morishita et al. 2003, 2008). To
462 efficiently assess the contribution of apatite on the electrical conductivity of the
463 phlogopite–apatite–peridotite rock system, three typical petrological average schemes
464 including the parallel, Hashin–Shtrikman upper bound and average models were
465 selected to calculate the electrical conductivity of sample at temperature range of
466 973–1373 K and 2.0 GPa. As noted by Xu et al. (2000), the parallel model stands for
467 the maximum value among the petrological average schemes from the laboratory–
468 based electrical conductivity results on three–phase (or two–phase) system at high
469 temperature and high pressure. A detailed parallel model (σ_P) can be described as,

470 $$\sigma_P = f_{Ap}\sigma_{Ap} + f_{Phl}\sigma_{Phl} + f_{Peri}\sigma_{Peri} \quad (9)$$

471 where f_{Ap}, f_{Phl} and f_{Peri} are the volume fractions of apatite single crystal, phlogopite
472 single crystal and peridotite, respectively; Ap, Phl and Peri represent apatite single
473 crystal, phlogopite single crystal and peridotite, respectively; σ_{Ap}, σ_{Phl} and σ_{Peri} are the
474 electrical conductivity of apatite single crystal, phlogopite single crystal and peridotite,

Always consult and cite the final, published document. See http:/www.minsocam.org or GeoscienceWorld

This is the peer-reviewed, final accepted version for American Mineralogist, published by the Mineralogical Society of America.
The published version is subject to change. Cite as Authors (Year) Title. American Mineralogist, in press.
DOI: https://doi.org/10.2138/am-2022-8900. http://www.minsocam.org/

475 respectively.

476 The middle Hashin–Shtrikman upper bound model (σ_{HS+}) is an efficient
477 petrological average scheme to fit and calculate the electrical conductivity results of
478 three–phase (or two–phase) system (Hashin and Shtrikman 1962; Hu et al. 2022a),
479 which is described as,

480 $$\sigma_{HS+} = \sigma_{Phl} + \frac{A_1}{1 - A_1(3\sigma_{Phl})^{-1}} \quad (10)$$

481 $$A_1 = \frac{f_{Ap}}{(\sigma_{Ap} - \sigma_{Phl})^{-1} + (3\sigma_{Phl})^{-1}} + \frac{f_{Peri}}{(\sigma_{Peri} - \sigma_{Phl})^{-1} + (3\sigma_{Phl})^{-1}} \quad (11)$$

482 As usual, the lower average model (σ_A) is adopted to transform the electrical
483 conductivity results of three constituent mineral single crystals (or two mineral single
484 crystals) into the electrical conductivity of rock system (Dai and Karato 2014a; Dai et
485 al. 2018a). Detailed average model for three–phase (or two–phase) system is exhibited
486 as follows,

487 $$\sigma_A = \frac{\sigma_P + \sigma_S + \sqrt{(\sigma_P + \sigma_S)^2 + 32\sigma_P\sigma_S}}{8} \quad (12)$$

488 $$\sigma_S = \frac{f_{Ap}\sigma_{Phl}\sigma_{Peri} + f_{Phl}\sigma_{Ap}\sigma_{Peri} + f_{Peri}\sigma_{Ap}\sigma_{Phl}}{\sigma_{Ap}\sigma_{Phl}\sigma_{Peri}} \quad (13)$$

489 where σ_P is the parallel model for the electrical conductivity of the phlogopite–
490 apatite–peridotite rock system from equation (9); σ_S is the series model for the
491 electrical conductivity of the phlogopite–apatite–peridotite rock system.

492 Figure 10 shows the functional dependence relation for the volume percentages
493 of apatite ranging from 1% to 10% on the electrical conductivity of the phlogopite–
494 apatite–peridotite rock system under three controlled petrological average schemes at
495 temperature range of 973–1373 K and 2.0 GPa. Wherein, the electrical conductivity

Always consult and cite the final, published document. See http:/www.minsocam.org or GeoscienceWorld

This is the peer-reviewed, final accepted version for American Mineralogist, published by the Mineralogical Society of America.
The published version is subject to change. Cite as Authors (Year) Title. American Mineralogist, in press.
DOI: https://doi.org/10.2138/am-2022-8900. http://www.minsocam.org/

496 of apatite is chosen from the average model of our present obtained anisotropic
497 electrical conductivity results. In order to profoundly illustrate the variation of volume
498 percentage on the electrical conductivity of the phlogopite–apatite–peridotite rock
499 system, previously classic electrical conductivity results on phlogopite single crystals
500 reported by Li et al. (2016) and dry peridotite originated from Dai et al. (2008) were
501 also adopted. As a whole, with increasing temperature, the electrical conductivity of
502 the phlogopite–apatite–peridotite rock system increases at each fixed petrological
503 average scheme, accordingly. Under conditions of three typical temperature points
504 (i.e., 973 K, 1173 K and 1373 K) and a constant volume percentage, the electrical
505 conductivity of the phlogopite–apatite–peridotite rock system of Hashin–Shtrikman
506 upper bound model (σ_{HS+}) is slightly lower than that of parallel model (σ_P), and ~2.8
507 times higher than that of average model (σ_A). As far as different petrological average
508 schemes, the electrical conductivity of the phlogopite–apatite–peridotite rock system
509 exhibits a similar tendency with the variation of volume percentages for apatite, i.e.
510 the electrical conductivity of the phlogopite–apatite–peridotite rock system increases
511 with the reduction in the content of apatite.

512 For a typical Hashin–Shtrikman upper bound model, the electrical conductivity–
513 depth profile for peridotite containing the 10% volume percentage of apatite was
514 established by converting the conductivity–temperature data into conductivity–depth
515 results. At the same time, the electrical conductivity results on other three
516 representative volatile–bearing metasomatism mineral single crystals (i.e., phlogopite,

Always consult and cite the final, published document. See http:/www.minsocam.org or GeoscienceWorld

This is the peer-reviewed, final accepted version for American Mineralogist, published by the Mineralogical Society of America.
The published version is subject to change. Cite as Authors (Year) Title. American Mineralogist, in press.
DOI: https://doi.org/10.2138/am-2022-8900. http://www.minsocam.org/

517 lawsonite and amphibole) were also compared in detail. The electrical conductivity
518 results on the single crystals of phlogopite, lawsonite and amphibole originated from
519 Li et al. (2016), Manthilake et al. (2015) and Hu et al. (2018), respectively. In order to
520 simplify the electrical conductivity–depth profile model, some indispensable
521 assumptions and extrapolations were proposed as follows, (1) the effects from water
522 of VMMs either the existing species of hydroxyl (i.e., apatite, phlogopite and
523 amphibole) or molecular structure (lawsonite) on the electrical conductivity of
524 peridotite containing the volume percentage of 10% VMMs, and their corresponding
525 partitioning coefficients between VMMs (i.e., apatite, phlogopite, amphibole and
526 lawsonite) and peridotite are inevitable, however, they are beyond our present
527 research range; (2) a feeble influence of pressure on the electrical conductivity of
528 apatite was observed ranging from 1.0 GPa to 3.0 GPa in the present study, which was
529 ignored during the construction of electrical conductivity–depth profile; (3) our
530 present high–temperature and high–pressure impedance spectroscopy measurements
531 were conducted under the control of Ni–NiO solid buffer, which was employed to
532 represent the oxygen fugacity in the upper Earth mantle (Dai et al. 2013); (4)
533 previously available results have indicated that grain boundary electrical conductivity
534 is negligible when compared with grain interior electrical conductivity and total
535 electrical conductivity (Dai et al. 2008; Yang and Heidelbach 2012), and thus, we
536 need not consider the influence of grain boundary on the electrical conductivity for
537 the system of the peridotite plus the individual VMMs (i.e., apatite, phlogopite,

Always consult and cite the final, published document. See http:/www.minsocam.org or GeoscienceWorld

This is the peer-reviewed, final accepted version for American Mineralogist, published by the Mineralogical Society of America.
The published version is subject to change. Cite as Authors (Year) Title. American Mineralogist, in press.
DOI: https://doi.org/10.2138/am-2022-8900. http://www.minsocam.org/

538 amphibole and lawsonite); (5) the chemical compositions of dry peridotite from Dai et
539 al. (2008), and four typical volatile–bearing metasomatism mineral single crystals for
540 phlogopite from Li et al. (2016), lawsonite from Manthilake et al. (2015), amphibole
541 from Hu et al. (2018), as well as our present measured apatite with its corresponding
542 stoichiometric composition of $Ca_{5.25}(PO_4)_3F_{1.23}Cl_{0.05}$ were adopted to represent the
543 mineralogical compositions of peridotite and various VMMs in western Junggar of
544 Xinjiang autonomous region, respectively, and the volume percentage of each VMM
545 in the dry peridotite is fixed at 10%; (6) the electrical conductivity results of peridotite
546 and various VMMs were properly extended on the basis of their respective electrical
547 conductivity–temperature dependence relation, as well as previously observed
548 temperature–induced dehydration of lawsonite from Manthilake et al. (2015) and
549 oxidation–dehydrogenation reaction of amphibole from Hu et al. (2018) were fully
550 considered; (7) previously available geothermal results suggested that the geothermal
551 gradients in western Junggar of Xinjiang autonomous region fall within the range of
552 11.6–27.6 K/km (Rao et al. 2013), therefore, we adopted 11.6 K/km and 27.6 K/km to
553 stand for the lower boundary and upper boundary of geothermal gradients in the
554 western Junggar of Xinjiang autonomous region, respectively; (8) except for our
555 present detailed investigation on the orientation–related electrical conductivity of
556 apatite, some representative high–conductivity accessory minerals (such as magnetite,
557 chromite and ilmenite) have an important influence on the electrical conductivity of
558 dry peridotite (or olivine polycrystalline aggregates), which have been deeply

Always consult and cite the final, published document. See http:/www.minsocam.org or GeoscienceWorld

This is the peer-reviewed, final accepted version for American Mineralogist, published by the Mineralogical Society of America.
The published version is subject to change. Cite as Authors (Year) Title. American Mineralogist, in press.
DOI: https://doi.org/10.2138/am-2022-8900. http://www.minsocam.org/

559 investigated in our recently reported results (Dai et al. 2019; Sun et al. 2021, 2022),
560 thus, we need not consider them in this study.

561 Figure 11 displays the electrical conductivity–depth profile of peridotite
562 containing the 10% volume percentage of apatite under two geothermal gradients of
563 11.6 K/km and 27.6 K/km at depth range of 20–90 km. Previously available results
564 for the field MT data in western Junggar of Xinjiang autonomous region from Zhang
565 et al. (2017) and Xu et al. (2020), as well as the electrical conductivity results for other
566 three VMMs (i.e., phlogopite, amphibole and lawsonite) are comprehensively
567 considered. As a whole, the electrical conductivity of peridotite containing the 10%
568 volume percentage of apatite increases gradually with the depth under two
569 representative geothermal gradients of 11.6 K/km and 27.6 K/km. For the electrical
570 conductivity of peridotite containing the 10% volume percentage of lawsonite, an
571 abrupt change is observed at depths of ~30 km and ~76 km for the corresponding
572 geothermal gradients of 27.6 K/km and 11.6 K/km, respectively, which can be
573 resulted in by the temperature–induced dehydration effect of lawsonite. The electrical
574 conductivity of peridotite containing the 10% volume percentage of amphibole also
575 exhibits a sudden discontinuity at the temperature of ~873 K due to the oxidation–
576 dehydrogenation reaction of amphibole. At a certain depth, when the geothermal
577 gradient is increased from the lower boundary of 11.6 K/km to the upper boundary of
578 27.6 K/km, there exists the differentiation of ~4 orders of magnitude in the electrical
579 conductivity of the 10% volume percentage of VMMs–containing peridotite. At a

Always consult and cite the final, published document. See http:/www.minsocam.org or GeoscienceWorld

This is the peer-reviewed, final accepted version for American Mineralogist, published by the Mineralogical Society of America.
The published version is subject to change. Cite as Authors (Year) Title. American Mineralogist, in press.
DOI: https://doi.org/10.2138/am-2022-8900. http://www.minsocam.org/

580 constant geothermal gradient, the electrical conductivity of peridotite containing the
581 10% volume percentage of apatite is lower than those of peridotite containing other
582 various 10% volume percentage of VMMs (i.e., phlogopite, lawsonite and amphibole),
583 and their conductivity–depth curves gradually converge with increasing depth. For the
584 lower boundary geothermal gradient of 11.6 K/km in the western Junggar of Xinjiang
585 autonomous region, it is evident that the electrical conductivity of peridotite with the
586 10% volume percentage of apatite is close to ~10^{-2} S/m at a depth of 90 km, which is
587 lower than that of the high conductivity zone. Therefore, the presence of the 10%
588 volume percentage of apatite in peridotite cannot explain the high conductivity
589 anomalies at a low geothermal gradient of 11.6 K/km, which may be closely related to
590 the presences of phlogopite and lawsonite. As far as the upper boundary geothermal
591 gradient of 27.6 K/km in the western Junggar of Xinjiang autonomous region, the
592 electrical conductivity of peridotite with the 10% volume percentage of apatite
593 reaches ~$10^{-1.8}$ S/m at a depth of ~40 km, which corresponds to the highest
594 measurement temperature of 1373 K in this study. The maximum electrical
595 conductivity of peridotite containing the 10% volume percentage of apatite is also
596 slightly lower than that of the high conductivity zone. Thus, the presence of the 10%
597 volume percentage of apatite in peridotite still cannot explain the high conductivity
598 anomalies at the geothermal gradient of 27.6 K/km, which may be closely related to
599 the presences of phlogopite, lawsonite and amphibole. In summary, the presence of
600 apatite in peridotite cannot explain the high conductivity anomalies for the lower

Always consult and cite the final, published document. See http:/www.minsocam.org or GeoscienceWorld

This is the peer-reviewed, final accepted version for American Mineralogist, published by the Mineralogical Society of America.
The published version is subject to change. Cite as Authors (Year) Title. American Mineralogist, in press.
DOI: https://doi.org/10.2138/am-2022-8900. http://www.minsocam.org/

601 boundary of 11.6 K/km and upper boundary of 27.6 K/km in western Junggar of
602 Xinjiang autonomous region, it can provide a reasonable constraint on those of
603 apatite–rich areas with relativity high resistivity.

604 Although our present obtained anisotropic electrical conductivity results of
605 apatite single crystals cannot explain the high conductivity anomalies, it is crucial to
606 deeply understand the geological cycle of halogen family element in the deep interior.
607 As the most important endmember among phosphate minerals, fluorapatite contains a
608 large number of volatile components. Previously available geological evidences have
609 already confirmed that the average concentration of fluorine element in the deep
610 Earth′s crust is approximate to 800 ppm wt, which mainly existed as the fluorine–rich
611 minerals of apatite and fluorspar (Barth 1947). As a predominated fluorine–bearing
612 phosphate mineral, apatite is widely distributed in a large number of basic–acid
613 igneous rocks (e.g., basalt, gabbro, granite, etc.) and regional metamorphic rocks (e.g.,
614 schist, gneiss, carbonaceous slate, etc.). In the recent several years, in order to explain
615 the high electrical conductivity anomalies in some representative geotectonic units of
616 the Tibetan Plateau, southern India and Dabie–Sulu ultrahigh–pressure metamorphic
617 belt, there are a large quantity of electrical conductivity results to be reported on those
618 of basic–acid igneous rocks and regional thermal metamorphic rocks under high–
619 temperature and high–pressure conditions (Dai et al. 2014, 2015, 2018b; Sun et al.
620 2019a, b, c). In comprehensive consideration of our present obtained anisotropic
621 electrical conductivity results on apatite at high temperature and high pressure, it is

Always consult and cite the final, published document. See http:/www.minsocam.org or GeoscienceWorld

This is the peer-reviewed, final accepted version for American Mineralogist, published by the Mineralogical Society of America.
The published version is subject to change. Cite as Authors (Year) Title. American Mineralogist, in press.
DOI: https://doi.org/10.2138/am-2022-8900. http://www.minsocam.org/

622 crucial to deeply understand the geochemical cycle of fluorine element in the deep
623 interior of the Earth. In addition, owing to the unique chemical and mineralogical
624 compositions for the existence of multi–component magmatic volatiles (e.g., fluorine,
625 chlorine and hydroxyl) in apatite, it is extremely widely applied in the field of many
626 regional magmatic hydrothermal deposits, such as the porphyry–type copper deposit
627 in the region of the American southwestern New Mexico, the porphyry–skarn type of
628 gold–copper deposit in the region of the Chinese southwestern Ailaoshan–Red River
629 belt and the porphyry–skarn type of iron–gold–copper deposit in the region of the
630 southern Peru's Andahuaylas–Yauri batholith (Huang et al. 2023). As a crucial
631 mineralization tracer, all of these volatile–related parameters including fluorine
632 content, chlorine content, as well as the ratio of fluorine and chlorine in apatite can be
633 used to efficiently explain the petrogenetic–metallogenic mechanism during the deep–
634 related fluid exsolution processes in the regions of synsubduction, continental
635 collision and intracontinental environments (Huang et al. 2023). Whereas, it is well
636 known that the electrical conductivity of relevant minerals and rocks is also highly
637 sensitive to the variations of volatile content at high temperature and high pressure. In
638 conclusion, more and more researches on high–pressure electrical conductivity
639 experiments for those of apatite family minerals are indispensable to be deeply
640 investigated in the future.

Always consult and cite the final, published document. See http:/www.minsocam.org or GeoscienceWorld

This is the peer-reviewed, final accepted version for American Mineralogist, published by the Mineralogical Society of America.
The published version is subject to change. Cite as Authors (Year) Title. American Mineralogist, in press.
DOI: https://doi.org/10.2138/am-2022-8900. http://www.minsocam.org/

641 # Acknowledgments

642 We thank Professor Geeth Manthilake from Laboratoire Magmas et Volcans,
643 National Center for Scientific Research, France, another one anonymous reviewer and
644 editor of Mainak Mookherjee from Earth Materials Laboratory, Department of Earth,
645 Ocean and Atmospheric Sciences, Florida State University, USA for their very helpful
646 comments and suggestions in the reviewing process, which helped us greatly in
647 improving the manuscript. Some beneficial discussions for the error analysis of
648 electron microprobe measurements in apatite single crystal were conducted with Dr.
649 Li Xiang from State Key Laboratory of Ore-Deposit Geochemistry, Institute of
650 Geochemistry, CAS. The native English speaker of Professor Sathiyadhas Sahaya
651 Jude Dhas from Department of Physics, Kings Engineering College, India was
652 appreciated to provide a professional help in the English improvements of revised
653 manuscript. In addition, we are very grateful to the advanced English editing service of
654 AJE (American Journal Experts) company for their great helps in English expression
655 style and writing skill in the final edition. This research was financially supported by
656 the NSF of China (grant numbers 42072055 and 42274137) and the Youth Innovation
657 Promotion Association of CAS (grant number 2019390).

658

Always consult and cite the final, published document. See http:/www.minsocam.org or GeoscienceWorld

This is the peer-reviewed, final accepted version for American Mineralogist, published by the Mineralogical Society of America.
The published version is subject to change. Cite as Authors (Year) Title. American Mineralogist, in press.
DOI: https://doi.org/10.2138/am-2022-8900. http://www.minsocam.org/

References

Barth, T.F. (1947) On the geochemical cycle of fluorine. The Journal of Geology, 55, 5, 420–426.

Brenan, J. (1994) Kinetics of fluorine, chlorine and hydroxyl exchange in fluorapatite. Chemical Geology, 110, 195–210.

Brunet, F., Allan, D.R., Redfern, S.A.T., Angel, R.J., Miletich, R., Reichmann, H.J., Sergent, J., and Hanfland, M. (1999) Compressibility and thermal expansivity of synthetic apatites, $Ca_5(PO_4)_3X$ with X = OH, F and Cl. European Journal of Mineralogy, 11, 1023–1035.

Cherniak, D.J. (2010a) Diffusion in carbonates, fluorite, sulfide minerals, and diamond. Reviews in Mineralogy and Geochemistry, 72, 871–897.

Cherniak, D.J. (2010b) Diffusion in accessory minerals: Zircon, titanite, apatite, monazite and xenotime. Reviews in Mineralogy and Geochemistry, 72, 1, 827–869.

Comodi, P., Liu, Y., Zanazzi, P.F., and Montagnoli, M. (2001a) Structural and vibrational behaviour of fluorapatite with pressure. Part I: in situ single-crystal X-ray diffraction investigation. Physics and Chemistry of Minerals, 28, 219–224.

Comodi, P., Liu, Y., and Frezzotti, M. L. (2001b) Structural and vibrational behaviour of fluorapatite with pressure. Part II: in situ micro-Raman spectroscopic investigation. Physics and Chemistry of Minerals, 28, 225–231.

Dai, L.D., and Karato, S. (2014a) High and highly anisotropic electrical conductivity of the asthenosphere due to hydrogen diffusion in olivine. Earth and Planetary Science Letters, 408, 79–86.

Dai, L.D., and Karato, S. (2014b) The effect of pressure on the electrical conductivity of olivine under the hydrogen-rich conditions. Physics of the Earth and Planetary Interiors, 232, 51–56.

Dai, L.D., and Karato, S. (2020) Electrical conductivity of Ti-bearing hydrous olivine

Always consult and cite the final, published document. See http:/www.minsocam.org or GeoscienceWorld

This is the peer-reviewed, final accepted version for American Mineralogist, published by the Mineralogical Society of America.
The published version is subject to change. Cite as Authors (Year) Title. American Mineralogist, in press.
DOI: https://doi.org/10.2138/am-2022-8900. http://www.minsocam.org/

686 aggregates at high temperature and high pressure. Journal of Geophysical
687 Research: Solid Earth, 125, e2020JB020309.
688 Dai, L.D., Li, H.P., Hu, H.Y., and Shan, S.M. (2008) Experimental study of grain
689 boundary electrical conductivities of dry synthetic peridotite under
690 high-temperature, high-pressure, and different oxygen fugacity conditions.
691 Journal of Geophysical Research: Solid Earth, 113, B12211.
692 Dai, L.D., Li, H.P., Hu, H.Y., Shan, S.M., Jiang, J.J., and Hui, K.S. (2012) The effect of
693 chemical composition and oxygen fugacity on the electrical conductivity of dry
694 and hydrous garnet at high temperatures and pressures. Contributions to
695 Mineralogy and Petrology, 163, 4, 689–700.
696 Dai, L.D., Li, H.P., Hu, H.Y., Jiang, J.J., Hui, K.S., and Shan, S.M. (2013) Electrical
697 conductivity of $Alm_{82}Py_{15}Grs_3$ almandine-rich garnet determined by impedance
698 spectroscopy at high temperatures and high pressures. Tectonophysics, 608, 1086–
699 1093.
700 Dai, L.D., Hu, H.Y., Li, H.P., Jiang, J.J., and Hui, K.S. (2014) Effects of temperature,
701 pressure and chemical composition on the electrical conductivity of granite and its
702 geophysical implications. American Mineralogist, 99, 1420–1428.
703 Dai, L.D., Jiang, J.J., Li, H.P., Hu, H.Y., and Hui, K.S. (2015) Electrical conductivity of
704 hydrous natural basalts at high temperatures and pressures. Journal of Applied
705 Geophysics, 112, 290–297.
706 Dai, L.D., Hu, H.Y., Li, H.P., Wu, L., Hui, K.S., Jiang, J.J., and Sun, W.Q. (2016)
707 Influence of temperature, pressure, and oxygen fugacity on the electrical
708 conductivity of dry eclogite, and geophysical implications. Geochemistry,
709 Geophysics, Geosystems, 17, 6, 2394–2407.
710 Dai, L.D., Hu, H.Y., Li, H.P., Sun, W.Q., and Jiang, J.J. (2018a) Influence of anisotropy
711 on the electrical conductivity and diffusion coefficient of dry K-feldspar:
712 Implications of the mechanism of conduction. Chinese Physics B, 27, 2, 028703.
713 Dai, L.D., Sun, W.Q., Li, H.P., Hu, H.Y., Wu, L., and Jiang, J.J. (2018b) Effect of

Always consult and cite the final, published document. See http:/www.minsocam.org or GeoscienceWorld

This is the peer-reviewed, final accepted version for American Mineralogist, published by the Mineralogical Society of America.
The published version is subject to change. Cite as Authors (Year) Title. American Mineralogist, in press.
DOI: https://doi.org/10.2138/am-2022-8900. http://www.minsocam.org/

714 chemical composition on the electrical conductivity of gneiss at high temperatures
715 and pressures. Solid Earth, 9, 233–245.
716 Dai, L.D., Hu, H.Y., Sun, W.Q., Li, H.P., Liu, C.C., and Wang, M.Q. (2019) Influence
717 of high conductive magnetite impurity on the electrical conductivity of dry olivine
718 aggregates at high temperature and high pressure. Minerals, 9, 44.
719 Dai, L.D., Hu, H.Y., He, Y., and Sun, W.Q. (2022) Some new progress in the
720 experimental measurements on electrical property of main minerals in the upper
721 mantle at high temperatures and high pressures. In Mineralogy edited by Miloš
722 René, IntechOpen, London, United Kingdom, pp. 15–38.
723 Evans, R.L., Hirth, G., Baba, K., Forsyth, D., Chave, A., and Makie, R. (2005)
724 Geophysical evidence from the MELT area for compositional control on oceanic
725 plates. Nature, 437, 249–252.
726 Efimov, A.A., Ronkin, Y.L., Malich, K.N., and Lepikhina, G.A. (2012) New Sm-Nd
727 and Rb-Sr (ID-TIMS) isotope data for apatite-phlogopite clinopyroxenites from
728 the dunite "Core" of the Konder Massif, Aldan Shield, Yakutia. Doklady Earth
729 Sciences, 445, 956–961.
730 Förster, M.W., and Selway, K. (2021) Melting of subducted sediments reconciles
731 geophysical images of subduction zones. Nature Communications, 12, 1320.
732 Griffin, W.L., Wass, S.Y., and Hollis, J.D. (1984) Ultramafic xenoliths from
733 Bullenmerri and Gnotuk maars, Victoria, Australia: Petrology of a subcontinental
734 crust-mantle transition. Journal of Petrology, 25, 53–87.
735 Hamilton, M.P., Jones, A.G., Evans, R.L., Evans, S., Fourie, C.J.S., Garcia, X.,
736 Mountford, A., and Spratt, J.E. (2006) Electrical anisotropy of South Africa
737 lithosphere compared with seismic anisotropy from shear-wave splitting analyses.
738 Physics of the Earth and Planetary Interiors, 158, 226–239.
739 Hashin, Z., and Shtrikman, S. (1962) A variational approach to the theory of the
740 effective magnetic permeability of multiphase materials. Journal of Applied
741 Physics, 33, 10, 3125–3131.

Always consult and cite the final, published document. See http:/www.minsocam.org or GeoscienceWorld

This is the peer-reviewed, final accepted version for American Mineralogist, published by the Mineralogical Society of America.
The published version is subject to change. Cite as Authors (Year) Title. American Mineralogist, in press.
DOI: https://doi.org/10.2138/am-2022-8900. http://www.minsocam.org/

742 Hong, M.L., Dai, L.D., Hu, H.Y., and Zhang, X.Y. (2022) Pressure-induced structural
743 phase transitions in natural kaolinite investigated by Raman spectroscopy and
744 electrical conductivity. American Mineralogist, 107, 385–394.
745 Hu, H.Y., Dai, L.D., Li, H.P., Hui, K.S., and Li, J. (2015) Temperature and high
746 pressure dependence of electrical conductivity in synthetic anorthite. Solid State
747 Ionics, 276, 136–141.
748 Hu, H.Y., Dai, L.D., Li, H.P., Hui, K.S., and Sun, W.Q. (2017) Influence of dehydration
749 on the electrical conductivity of epidote and implications for high conductivity
750 anomalies in subduction zones. Journal of Geophysical Research: Solid Earth, 122,
751 2751–2762.
752 Hu, H.Y., Dai, L.D., Li, H.P., Sun, W.Q., and Li, B.S. (2018) Effect of dehydrogenation
753 on the electrical conductivity of Fe-bearing amphibole: Implications for high
754 conductivity anomalies in subduction zones and continental crust. Earth and
755 Planetary Science Letters, 498, 27–37.
756 Hu, H.Y., Dai, L.D., Sun, W.Q., Wang, M.Q., and Jing, C.X. (2022a) Constraints on
757 fluids in the continental crust from laboratory-based electrical conductivity
758 measurements of plagioclase. Gondwana Research, 107, 1–12.
759 Hu, H.Y., Dai, L.D., Sun, W.Q., Zhuang, Y.K., Liu, K.X., Yang, L.F., Pu, C., Hong,
760 M.L., Wang, M.Q., Hu, Z.M., Jing, C.X., Li, C., Yin, C.Y., and Paramasivam, S.
761 (2022b) Some remarks on the electrical conductivity of hydrous silicate minerals
762 in the earth crust, upper mantle and subduction zone at high temperatures and high
763 pressures. Minerals, 12, 161.
764 Huang, M.L., Zhu, J.J., Chiaradia, M., Hu, R.Z., Xu, L.L., and Bi, X.W. (2023) Apatite
765 volatile contents of porphyry Cu deposits controlled by depth-related fluid
766 exsolution processes. Economic Geology, in press,
767 https://doi.org/10.5382/econgeo.5000.
768 Huebner, J.S., and Voigt, D.E. (1988) Electrical conductivity of diopside: Evidence for
769 oxygen vacancies. American Mineralogist, 73, 1235–1254.

Always consult and cite the final, published document. See http:/www.minsocam.org or GeoscienceWorld

This is the peer-reviewed, final accepted version for American Mineralogist, published by the Mineralogical Society of America.
The published version is subject to change. Cite as Authors (Year) Title. American Mineralogist, in press.
DOI: https://doi.org/10.2138/am-2022-8900. http://www.minsocam.org/

770 Huebner, J.S., and Dillenburg, R.G. (1995) Impedance spectra of hot, dry silicate
771 minerals and rock: Qualitative interpretation of spectra. American Mineralogist,
772 80, 46–64.
773 Konzett, J., and Frost, D.J. (2009) The high *P–T* stability of hydroxylapatite in natural
774 and simplified MORB–an experimental study to 15 GPa with implications for
775 transport and storage of phosphorus and halogens in subduction zones. Journal of
776 Petrology, 50, 2043–2062.
777 Li, W., Chakraborty, S., Nagashima, K., and Costa, F. (2020) Multicomponent diffusion
778 of F, Cl and OH in apatite with application to magma ascent rates. Earth and
779 Planetary Science Letters, 550, 116545.
780 Li, Y., Yang, X.Z., Yu, J.H., and Cai, Y.F. (2016) Unusually high electrical conductivity
781 of phlogopite: The possible role of fluorine and geophysical implications.
782 Contributions to Mineralogy and Petrology, 171, 37.
783 Li, Y., Jiang, H.T, and Yang, X.Z. (2017) Fluorine follows water: Effect on electrical
784 conductivity of silicate minerals by experimental constraints from phlogopite.
785 Geochimica et Cosmochimica Acta, 217, 16–27.
786 Liu, Y., Junge, A., Yang, B., Löwer, A., Cembrowski, M., and Xu, Y.X. (2019a)
787 Electrically anisotropic crust from three–dimensional magnetotelluric modeling in
788 the western Junggar, NW China. Journal of Geophysical Research: Solid Earth,
789 124, 9474–9494.
790 Liu, H.Y., Zhu, Q., and Yang, X.Z. (2019b) Electrical conductivity of fluorite and
791 fluorine conduction. Minerals, 9, 72.
792 Manthilake, G., Mookherjee, M., Bolfan–Casanova, N., and Andrault, D. (2015)
793 Electrical conductivity of lawsonite and dehydrating fluids at high pressures and
794 temperatures. Geophysical Research Letters, 42, 18, 7398–7405.
795 Manthilake, G., Bolfan–Casanova, N., Novella, D., Mookherjee, M., and Andrault, D.
796 (2016) Dehydration of chlorite explains anomalously high electrical conductivity
797 in the mantle wedges. Science Advances, 2, e1501631.

Always consult and cite the final, published document. See http:/www.minsocam.org or GeoscienceWorld

This is the peer-reviewed, final accepted version for American Mineralogist, published by the Mineralogical Society of America.
The published version is subject to change. Cite as Authors (Year) Title. American Mineralogist, in press.
DOI: https://doi.org/10.2138/am-2022-8900. http://www.minsocam.org/

798 Manthilake, G., Koga1, K.T., Ye, P., and Mookherjee, M. (2021a) Halogen bearing
799 amphiboles, aqueous fluids, and melts in subduction zones: Insights on halogen
800 cycle from electrical conductivity. Journal of Geophysical Research: Solid Earth,
801 126, 3, 021339.
802 Manthilake, G., Ye, P., Koga1, K.T., and Mookherjee, M. (2021b) Tracking slab surface
803 temperatures with electrical conductivity of glaucophane. Scientific Reports, 11,
804 18014.
805 Marocchi, M., Mair, V., Tropper, P., and Bargossi, G.M. (2009) Metasomatic reaction
806 bands at the Mt. Hochwart gneiss-peridotite contact (Ulten Zone, Italy): Insights
807 into fluid-rock interaction in subduction zones. Mineralogy and Petrology, 95,
808 251–272.
809 Matsukage, K.N., Ono, S., Kawamoto, T., and Kikegawa, T. (2004) The
810 compressibility of a natural apatite. Physics and Chemistry of Minerals, 31, 580–
811 584.
812 McKenzie, D., and Bickle, M.J. (1988) The volume and composition of melt generated
813 by extension of the lithosphere. Journal of Petrology, 29, 625–679.
814 Morishita, T., Araic, S., and Tamura, A. (2003) Petrology of an apatite-rich layer in
815 the Finero phlogopite–peridotite, Italian Western Alps; implications for evolution
816 of a metasomatising agent. Lithos, 69, 37–49.
817 Morishita, T., Hattori, K.H., Terada, K., Matsumoto, T., Yamamoto, K., Takebe, M.,
818 Ishida, Y., Tamura, A., and Arai, S. (2008) Geochemistry of apatite-rich layers in
819 the Finero phlogopite–peridotite massif (Italian Western Alps) and ion microprobe
820 dating of apatite. Chemical Geology, 251, 99–111.
821 Murayama, J.K., Nakai, S., Kato, M., and Kumazawa, M. (1986) A dense polymorph of
822 $Ca_3(PO_4)_2$: A high pressure phase of apatite decomposition and its geochemical
823 significance. Physics of the Earth and Planetary Interiors, 44, 293–303.
824 Naif, S., Key, K., Constable, S., and Evans, R.L. (2013) Melt-rich channel observed at
825 the lithosphere–asthenosphere boundary. Nature, 495, 356–359.

Always consult and cite the final, published document. See http:/www.minsocam.org or GeoscienceWorld

This is the peer-reviewed, final accepted version for American Mineralogist, published by the Mineralogical Society of America.
The published version is subject to change. Cite as Authors (Year) Title. American Mineralogist, in press.
DOI: https://doi.org/10.2138/am-2022-8900. http://www.minsocam.org/

O'Reilly, S.Y. (1987) Volatile-rich mantle beneath eastern Australia. In: Nixon, P. H. (Ed.), Mantle Xenoliths. Wiley London, pp. 661–670.

O'Reilly, S.Y., and Griffin, W.L. (2000) Apatite in the mantle: Implications for metasomatic processes and high heat production in Phanerozoic mantle. Lithos, 53, 217–232.

Özaydın, S., and Selway, K. (2022) The relationship between kimberlitic magmatism and electrical conductivity anomalies in the mantle. Geophysical Research Letters, 49, e2022GL099661.

Rao, S., Hu, S.B., Zhu, C.Q., Tang, X.Y., Li, W.W., and Wang, J.Y. (2013) The characteristics of heat flow and lithospheric thermal structure in Junggar basin, northwest China. Chinese Journal of Geophysics, 56, 2760–2770.

Roden, M.F., Frey, F.A., and Francis, D.M. (1984) An example of consequent mantle metasomatism in peridotite inclusions from Nunivak Island, Alaska. Journal of Petrology, 2, 546–577.

Saltas, V., Chatzistamou, V., Pentari, D., Paris, E., Triantis, D., Fitilis, I., and Vallianatos, F. (2013) Complex electrical conductivity measurements of a KTB amphibolite sample at elevated temperatures. Materials Chemistry and Physics, 139, 169–175.

Saltas, V., Pentari, D., and Vallianatos, F. (2020) Complex electrical conductivity of biotite and muscovite micas at elevated temperatures: A comparative study. Materials, 13, 3513.

Selway, K. (2014) On the causes of electrical conductivity anomalies in tectonically stable lithosphere. Surveys in Geophysics, 35, 219–257.

Selway, K. (2015) Negligible effect of hydrogen content on plate strength in East Africa. Nature Geoscience, 10, 1038.

Selway, K. (2019) Electrical discontinuities in the continental lithosphere imaged with magnetotellurics. In: Lithospheric Discontinuities, 239, AGU Geophysical Monograph edited by Huaiyu Yuan and Barbara Romanowicz, pp. 89–110.

Always consult and cite the final, published document. See http:/www.minsocam.org or GeoscienceWorld

This is the peer-reviewed, final accepted version for American Mineralogist, published by the Mineralogical Society of America.
The published version is subject to change. Cite as Authors (Year) Title. American Mineralogist, in press.
DOI: https://doi.org/10.2138/am-2022-8900. http://www.minsocam.org/

Selway, K., and O'Donnell, J.P. (2019) A small, unextractable melt fraction as the cause for the low velocity zone. Earth and Planetary Science Letters, 517, 117–124.

Selway, K., O'Donnell, J.P., and Özaydin, S. (2019) Upper mantle melt distribution from petrologically constrained magnetotellurics. Geochemistry, Geophysics, Geosystems, 20, 3328–3346.

Shannon, R.D. (1976) Revised effective ionic radii and systematic studies of interatomic distances in halides and chalcogenides. Acta Crystallographica, Section A, 32, 751–767.

Simpson, F., and Tommasi, A. (2005) Hydrogen diffusivity and electrical anisotropy of a peridotite mantle. Geophysical Journal International, 160, 1092–1102.

Sivakumar, A., Suresh, S., Pradeep, J.A., Balachandar, S., and Martin Britto Dhas, S.A. (2018) Effect of shock waves on dielectric properties of KDP crystal. Journal of Electronic Materials, 47, 4831–4839.

Sivakumar, A., Dhas, S.S.J., Almansour, A.I., Kumar, R.S., Arumugam, N., Prabhu, S., Sivashanmugan, K., Ramesh, R., and Martin Britto Dhas, S.A. (2021) Shock waves induced enhancement of electrochemical properties of $CoFe_2O_4$ nanoparticles for energy storage applications. Surfaces and Interfaces, 27, 101539.

Sivakumar, A., Mowlika, V., Dhas, S.S.J., Prabhu, S., Ramesh, R., Robert, R., and Martin Britto Dhas, S.A. (2022) Shock wave induced switchable electrical resistance of $ZnFe_2O_4$ nanoparticles. Solid State Sciences, 125, 106843.

Sun, W.Q., Dai, L.D., Li, H.P., Hu, H.Y., Wu, L., and Jiang, J.J. (2017) Electrical conductivity of mudstone (before and after dehydration at high *P–T*) and a test of high conductivity layers in the crust. American Mineralogist, 102, 2450–2456.

Sun, W.Q., Dai, L.D., Li, H.P., Hu, H.Y., and Liu, C.C. (2019a) Effect of temperature, pressure and chemical composition on the electrical conductivity of granulite and geophysical implications. Journal of Mineralogical and Petrological Sciences, 114, 87–98.

Sun, W.Q., Dai, L.D., Li, H.P., Hu, H.Y., Liu, C.C., and Wang, M.Q. (2019b) Effect of

Always consult and cite the final, published document. See http:/www.minsocam.org or GeoscienceWorld

This is the peer-reviewed, final accepted version for American Mineralogist, published by the Mineralogical Society of America.
The published version is subject to change. Cite as Authors (Year) Title. American Mineralogist, in press.
DOI: https://doi.org/10.2138/am-2022-8900. http://www.minsocam.org/

882 temperature, pressure and chemical compositions on the electrical conductivity of
883 schist: Implications for electrical structures under the Tibetan plateau. Materials,
884 12, 961.
885 Sun, W.Q., Dai, L.D., Li, H.P., Hu, H.Y., Jiang, J.J., and Liu, C.C. (2019c)
886 Experimental study on the electrical properties of carbonaceous slate: A special
887 natural rock with unusually high conductivity at high temperatures and pressures.
888 High Temperatures-High Pressures, 48, 455–467.
889 Sun, W.Q., Dai, L.D., Li, H.P., Hu, H.Y., Jiang, J.J., and Wang, M.Q. (2020) Electrical
890 conductivity of clinopyroxene–NaCl–H_2O system at high temperatures and
891 pressures: Implications for high-conductivity anomalies in the deep crust and
892 subduction zone. Journal of Geophysical Research: Solid Earth, 125,
893 e2019JB019093.
894 Sun, W.Q., Jiang, J.J., Dai, L.D., Hu, H.Y., Wang, M.Q., Qi, Y.Q., and Li, H.P. (2021)
895 Electrical properties of dry polycrystalline olivine mixed with various chromite
896 contents: Implications for the high conductivity anomalies in subduction zones.
897 Geoscience Frontiers, 12, 5, 101178.
898 Sun, W.Q., Dai, L.D., Hu, H.Y., Wang, M.Q., Hu, Z.M., and Jing, C.X. (2022)
899 Experimental research on electrical conductivity of the olivine–ilmenite system at
900 high temperatures and high pressures. Frontiers in Earth Sciences, 10, 681003.
901 Wang, K.L., Zhang, Y., and Naab, F.U. (2011) Calibration for IR absorbance
902 measurements of OH in apatite. American Mineralogist, 96, 1392–1397.
903 Xu, Y.S., Shankland, T.J., and Duba, A.G. (2000) Pressure effect on electrical
904 conductivity of mantle olivine. Physics of the Earth and Planetary Interiors, 118, 1,
905 149–161.
906 Xu, Y.X., Yang, B., Zhang, S., Liu, Y., Zhu, L.P., Huang, R., Chen, C., Li, Y.T., and Luo,
907 Y.H. (2016) Magnetotelluric imaging of a fossil Paleozoic intraoceanic subduction
908 zone in western Junggar, NW China. Journal of Geophysical Research: Solid
909 Earth, 121, 4103–4117.

Always consult and cite the final, published document. See http:/www.minsocam.org or GeoscienceWorld

This is the peer-reviewed, final accepted version for American Mineralogist, published by the Mineralogical Society of America.
The published version is subject to change. Cite as Authors (Year) Title. American Mineralogist, in press.
DOI: https://doi.org/10.2138/am-2022-8900. http://www.minsocam.org/

910 Xu, Y.X., Yang, B., Zhang, A.Q., Wu, S.C., Zhu, L., Yang, Y.J., Wang, Q.Y., and Xia,
911 Q.K. (2020) Magnetotelluric imaging of a fossil oceanic plate in northwestern
912 Xinjiang, China. Geology, 48, 4, 385–389.
913 Yang, X.Z. (2012) Orientation-related electrical conductivity of hydrous olivine,
914 clinopyroxene and plagioclase and implications for the structure of the lower
915 continental crust and uppermost mantle. Earth and Planetary Science Letters, 317–
916 318, 241–250.
917 Yang, X.Z., and McCammon, C. (2012) Fe^{3+}-rich augite and high electrical
918 conductivity in the deep lithosphere. Geology, 40, 2, 131–134.
919 Yang, X.Z., and Heidelbach, F. (2012) Grain size effect on the electrical conductivity of
920 clinopyroxene. Contributions to Mineralogy and Petrology, 163, 939–947.
921 Ye, P., Manthilake, G., and Mookherjee, M. (2022) Electrical conductivity of
922 metasomatized lithology in subcontinental lithosphere. American Mineralogist,
923 107, 413–420.
924 Zhang, S., Xu, Y.X., Jiang, L., Yang, B., Liu, Y., Griffin, W.L., Luo, Y., Huang, R.,
925 Zhou, Y., and Zhang, L.L. (2017) Electrical structures in the northwest margin of
926 the Junggar basin: Implications for its late Paleozoic geodynamics.
927 Tectonophysics, 717, 473–483.

Always consult and cite the final, published document. See http:/www.minsocam.org or GeoscienceWorld

This is the peer-reviewed, final accepted version for American Mineralogist, published by the Mineralogical Society of America.
The published version is subject to change. Cite as Authors (Year) Title. American Mineralogist, in press.
DOI: https://doi.org/10.2138/am-2022-8900. http://www.minsocam.org/

928 # Figure captions:

929 **Figure 1.** The optical microscopic observation (a) and the corresponding crystalline
930 structure (b) of apatite single crystal.

931 **Figure 2.** Fourier transform infrared (FT–IR) spectroscopy of apatite single crystals
932 before and after electrical conductivity measurements at the wavenumber range of
933 3000–4000 cm^{-1}. The water contents for starting and recovered samples were
934 calculated as 176.69 ppm wt and 134.87 ppm wt, respectively, which suggested no
935 clear water loss during the process of electrical conductivity measurements.

936 **Figure 3.** Cross–section diagram of the sample assemblage for high–pressure
937 impedance spectroscopy measurements.

938 **Figure 4.** Representative complex impedance spectra for apatite single crystal along
939 the [010] crystallographic orientation at conditions of 973–1373 K and 2.0 GPa.
940 Wherein, Z' and Z'' are the real and imaginary parts of the complex impedance
941 spectroscopy, respectively. An equivalent circuit composed of the series conjunction of
942 parallel R_S–CPE_S and parallel R_E–CPE_E was selected to fit the impedance semicircular
943 arc. R_S and CPE_S stand for the electrical resistance and the constant phase element of
944 the sample, respectively; R_E and CPE_E represent the electrical resistance and the
945 constant phase element from the polarization effect of the sample–electrode interface,
946 respectively.

947 **Figure 5.** Logarithmic electrical conductivity of apatite single crystal along the [001]
948 crystallographic orientation as a function of reciprocal temperature in two continuous
949 heating−cooling cycles at 973–1373 K and 3.0 GPa.

950 **Figure 6.** Influence of pressure on the electrical conductivity of apatite single crystals
951 along the [001] crystallographic orientation at temperature range of 973–1373 K.

Always consult and cite the final, published document. See http:/www.minsocam.org or GeoscienceWorld

This is the peer-reviewed, final accepted version for American Mineralogist, published by the Mineralogical Society of America.
The published version is subject to change. Cite as Authors (Year) Title. American Mineralogist, in press.
DOI: https://doi.org/10.2138/am-2022-8900. http://www.minsocam.org/

952 **Figure 7.** Electrical conductivity of apatite single crystals along three main [001],
953 [100] and [010] crystallographic orientations at conditions of 973–1373 K and 2.0
954 GPa. We also compared it with the fitting conductivity results by virtue of three
955 representative averaging schemes of series model (σ_S), parallel model (σ_P) and
956 average model (σ_A) in detail. The electrical conductivity of the background of
957 magnesium oxide is also included under conditions of wider temperature range from
958 1073 K to 1523 K and 2.0 GPa.

959 **Figure 8.** The degree of electrical conductivity anisotropy for apatite single crystal as
960 a function of temperature from 900 K to 1700 K, and the comparison with hydrous
961 olivine single crystal from Dai and Karato (2014a) and olivine with the 10% volume
962 percentage of apatite calculated using our present anisotropic electrical conductivity
963 data and Hashin–Shtrikman upper bound model. The brown region stands for the
964 temperature range of 1550–1650 K in the asthenosphere (McKenzie and Bickle 1988).
965 The blue region represents the degree of electrical conductivity anisotropy in the
966 asthenosphere by a factor of ~2–3 higher along the flow direction on the horizontal
967 plane (Evans et al. 2005; Naif et al. 2013). These conductivity anisotropy results for
968 the mineral single crystals can be transformed into the conductivity anisotropy of
969 anisotropic aggregates by using numerical research to be reported by Simpson and
970 Tommasi (2005).

971 **Figure 9.** Comparisons of the anisotropic electrical conductivity results of apatite
972 single crystals and other three VMMs (i.e., phlogopite, amphibole and lawsonite). The
973 lines are labeled as follows: (1) Black solid lines represent our present results for the
974 anisotropic electrical conductivity of apatite single crystals along three main [001],
975 [100] and [010] crystallographic orientations; (2) Blue dashed lines represent the
976 electrical conductivity of phlogopite along three main crystalline directions from Li et
977 al. (2016); (3) Green dashed line represents the electrical conductivity of lawsonite

Always consult and cite the final, published document. See http:/www.minsocam.org or GeoscienceWorld

This is the peer-reviewed, final accepted version for American Mineralogist, published by the Mineralogical Society of America.
The published version is subject to change. Cite as Authors (Year) Title. American Mineralogist, in press.
DOI: https://doi.org/10.2138/am-2022-8900. http://www.minsocam.org/

978 measured by Manthilake et al. (2015), as well as (4) Red dashed line represents the
979 electrical conductivity of iron–bearing amphibole single crystals investigated by Hu et
980 al. (2018).

981 **Figure 10.** Three typical petrological average schemes for the electrical conductivity
982 of the phlogopite–apatite–peridotite rock system with the variation of the volume
983 fractions of apatite ranging from 1% to 10% at temperatures of 973–1373 K and 2.0
984 GPa. All of these solid lines, dashed lines and dotted lines stand for the average model
985 (σ_A), Hashin–Shtrikman upper bound model (σ_{HS+}) and parallel model (σ_P) for the
986 electrical conductivity of the phlogopite–apatite–peridotite rock system, respectively.
987 Electrical conductivity data for apatite single crystals, phlogopite single crystals and
988 dry peridotite were adopted from the average model for our present anisotropic
989 electrical conductivity results, Li et al. (2016) and Dai et al. (2008), respectively.

990 **Figure 11.** Laboratory–based electrical conductivity–depth profile for peridotite
991 containing the 10% volume percentage of apatite on the basis of our average model
992 for the anisotropic electrical conductivity of apatite and two different geothermal
993 gradients of 11.6 K/km and 27.6 K/km at depth range of 20–90 km. The field MT data
994 in western Junggar of Xinjiang autonomous region from Zhang et al. (2017) and Xu et
995 al. (2020), as well as the previously reported electrical conductivity results for dry
996 peridotite reported by Dai et al. (2008), and other three VMMs of the mineral single
997 crystals (i.e., phlogopite, lawsonite and amphibole) from Li et al. (2016), Manthilake
998 et al. (2015) and Hu et al. (2018) are also included. Wherein, red and blue lines stand
999 for the upper boundary of 27.6 K/km and lower boundary of 11.6 K/km for the
1000 geothermal gradients in the western Junggar of Xinjiang autonomous region,
1001 respectively (Rao et al. 2013); solid, dotted, dash–dot and dashed lines stand for the
1002 electrical conductivity of peridotite containing the 10% volume percentage of apatite,
1003 peridotite containing the 10% volume percentage of phlogopite, peridotite containing

Always consult and cite the final, published document. See http:/www.minsocam.org or GeoscienceWorld

This is the peer-reviewed, final accepted version for American Mineralogist, published by the Mineralogical Society of America.
The published version is subject to change. Cite as Authors (Year) Title. American Mineralogist, in press.
DOI: https://doi.org/10.2138/am-2022-8900. http://www.minsocam.org/

1004 the 10% volume percentage of lawsonite and peridotite containing the 10% volume
1005 percentage of amphibole, respectively; the green region stands for the high
1006 conductivity zone with its electrical conductivity values of ~10^{-2}–1 S/m under the
1007 western Junggar of Xinjiang autonomous region at depths of 20–90 km (Xu et al.
1008 2020).

Always consult and cite the final, published document. See http:/www.minsocam.org or GeoscienceWorld

This is the peer-reviewed, final accepted version for American Mineralogist, published by the Mineralogical Society of America.
The published version is subject to change. Cite as Authors (Year) Title. American Mineralogist, in press.
DOI: https://doi.org/10.2138/am-2022-8900. http://www.minsocam.org/

1009 **TABLE 1.** Chemical compositions of the starting and recovered apatite single crystals before and
1010 after electrical conductivity measurements.

Compositions	Starting sample (wt.%)	Recovered sample (wt.%)
SiO_2	0.43 ± 0.05	0.37 ± 0.06
FeO	0.03 ± 0.01	0.02 ± 0.01
CaO	54.93 ± 0.05	54.88 ± 0.10
P_2O_5	39.55 ± 0.30	39.75 ± 0.16
SO_3	0.67 ± 0.03	0.64 ± 0.03
SrO	0.09 ± 0.02	0.08 ± 0.02
F	4.33 ± 0.02	4.36 ± 0.05
Cl	0.23 ± 0.01	0.24 ± 0.02
Ce_2O_3	0.43 ± 0.02	0.42 ± 0.07
Nd_2O_3	0.13 ± 0.03	0.16 ± 0.04
Total	98.99 ± 0.24	99.03 ± 0.30

1011

Always consult and cite the final, published document. See http:/www.minsocam.org or GeoscienceWorld

This is the peer-reviewed, final accepted version for American Mineralogist, published by the Mineralogical Society of America.
The published version is subject to change. Cite as Authors (Year) Title. American Mineralogist, in press.
DOI: https://doi.org/10.2138/am-2022-8900. http://www.minsocam.org/

1012 **TABLE 2.** Fitting parameters of the Arrhenius relation for the electrical conductivity of apatite

1013 single crystals along three main crystallographic orientations under conditions of 973–1373 K and

1014 1.0–3.0 GPa.

Run No.	Orientation	T (K)	P (GPa)	Log σ_0	ΔH (eV)	R^2	ΔU (eV)	ΔV
Ap01	[001]	973–1373	1.0	5.95 ± 0.33	2.14 ± 0.07	0.9911	–	–
Ap04	[001]	973–1373	2.0	6.12 ± 0.29	2.24 ± 0.06	0.9940	2.05 ± 0.06	9.31 ± 0.98
Ap06	[001]	973–1373	3.0	6.32 ± 0.20	2.33 ± 0.05	0.9972	–	–
Ap09	[100]	973–1373	2.0	3.85 ± 0.16	1.92 ± 0.04	0.9974	–	–
Ap10	[010]	973–1373	2.0	4.18 ± 0.19	2.04 ± 0.05	0.9967	–	–

1015

Always consult and cite the final, published document. See http:/www.minsocam.org or GeoscienceWorld

This is the peer-reviewed, final accepted version for American Mineralogist, published by the Mineralogical Society of America.
The published version is subject to change. Cite as Authors (Year) Title. American Mineralogist, in press.
DOI: https://doi.org/10.2138/am-2022-8900. http://www.minsocam.org/

Figure 1.

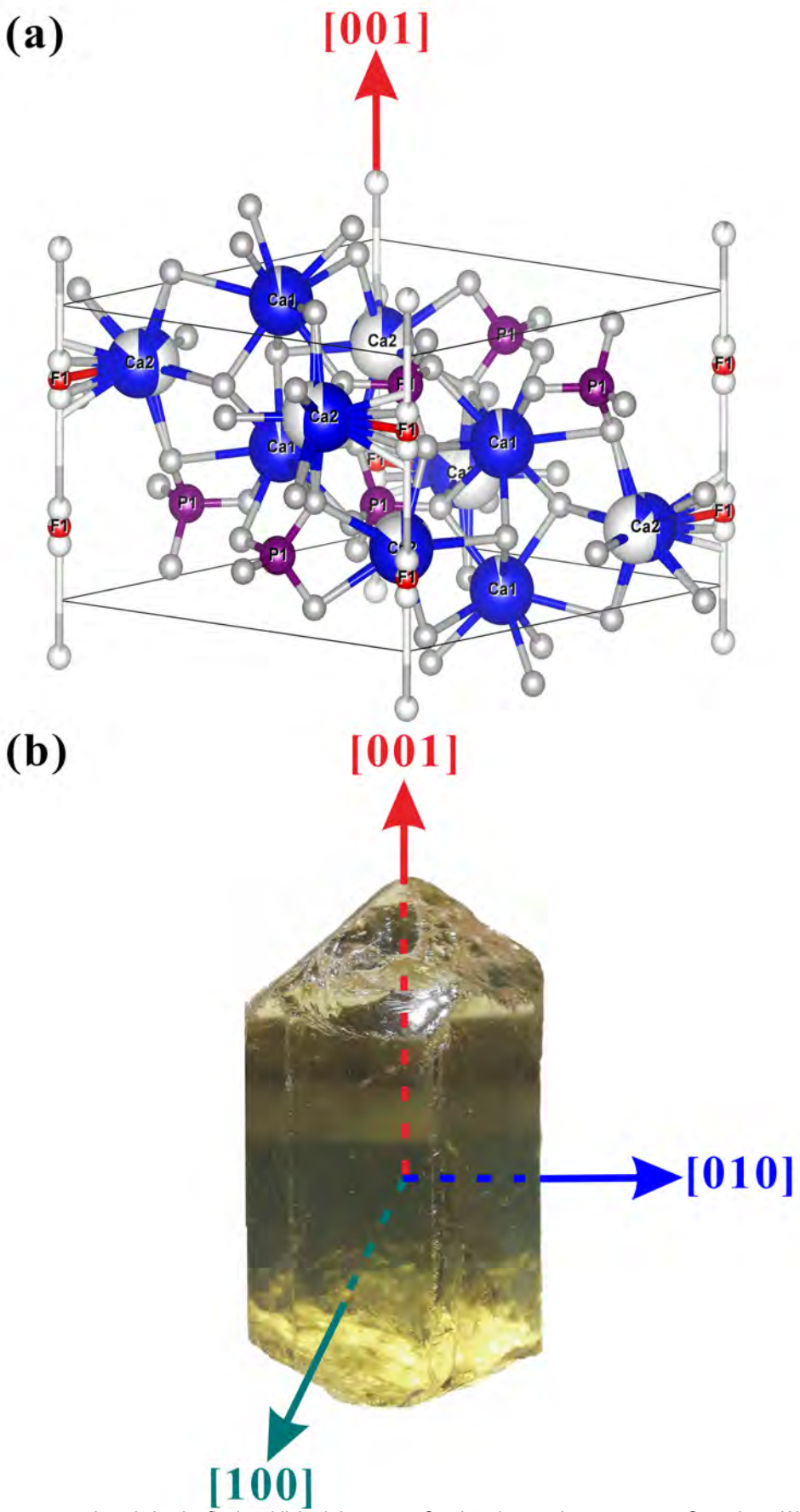

Always consult and cite the final, published document. See http:/www.minsocam.org or GeoscienceWorld

This is the peer-reviewed, final accepted version for American Mineralogist, published by the Mineralogical Society of America.
The published version is subject to change. Cite as Authors (Year) Title. American Mineralogist, in press.
DOI: https://doi.org/10.2138/am-2022-8900. http://www.minsocam.org/

Figure 2.

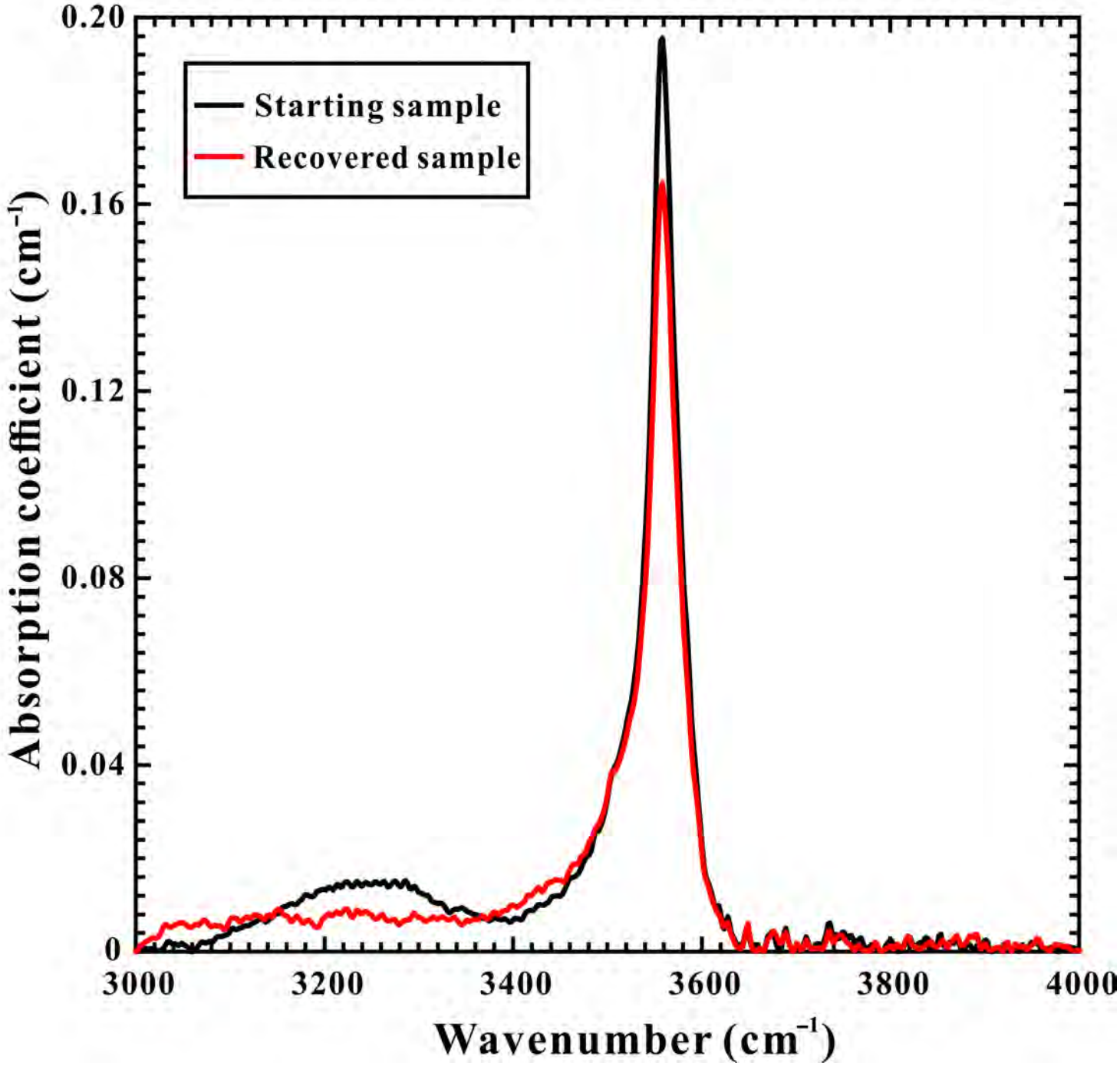

Always consult and cite the final, published document. See http:/www.minsocam.org or GeoscienceWorld

This is the peer-reviewed, final accepted version for American Mineralogist, published by the Mineralogical Society of America.
The published version is subject to change. Cite as Authors (Year) Title. American Mineralogist, in press.
DOI: https://doi.org/10.2138/am-2022-8900. http://www.minsocam.org/

Figure 3.

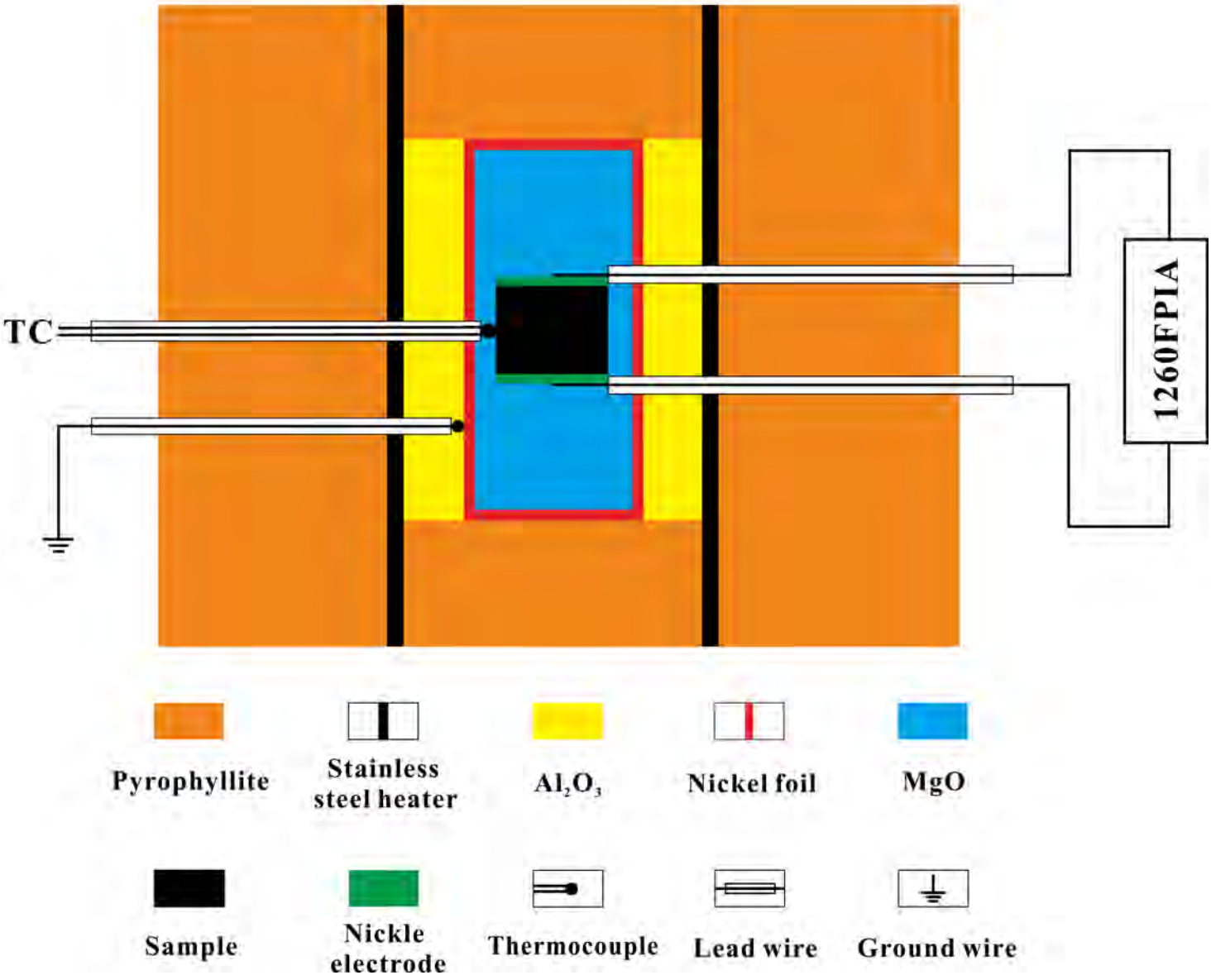

Always consult and cite the final, published document. See http:/www.minsocam.org or GeoscienceWorld

This is the peer-reviewed, final accepted version for American Mineralogist, published by the Mineralogical Society of America.
The published version is subject to change. Cite as Authors (Year) Title. American Mineralogist, in press.
DOI: https://doi.org/10.2138/am-2022-8900. http://www.minsocam.org/

Figure 4.

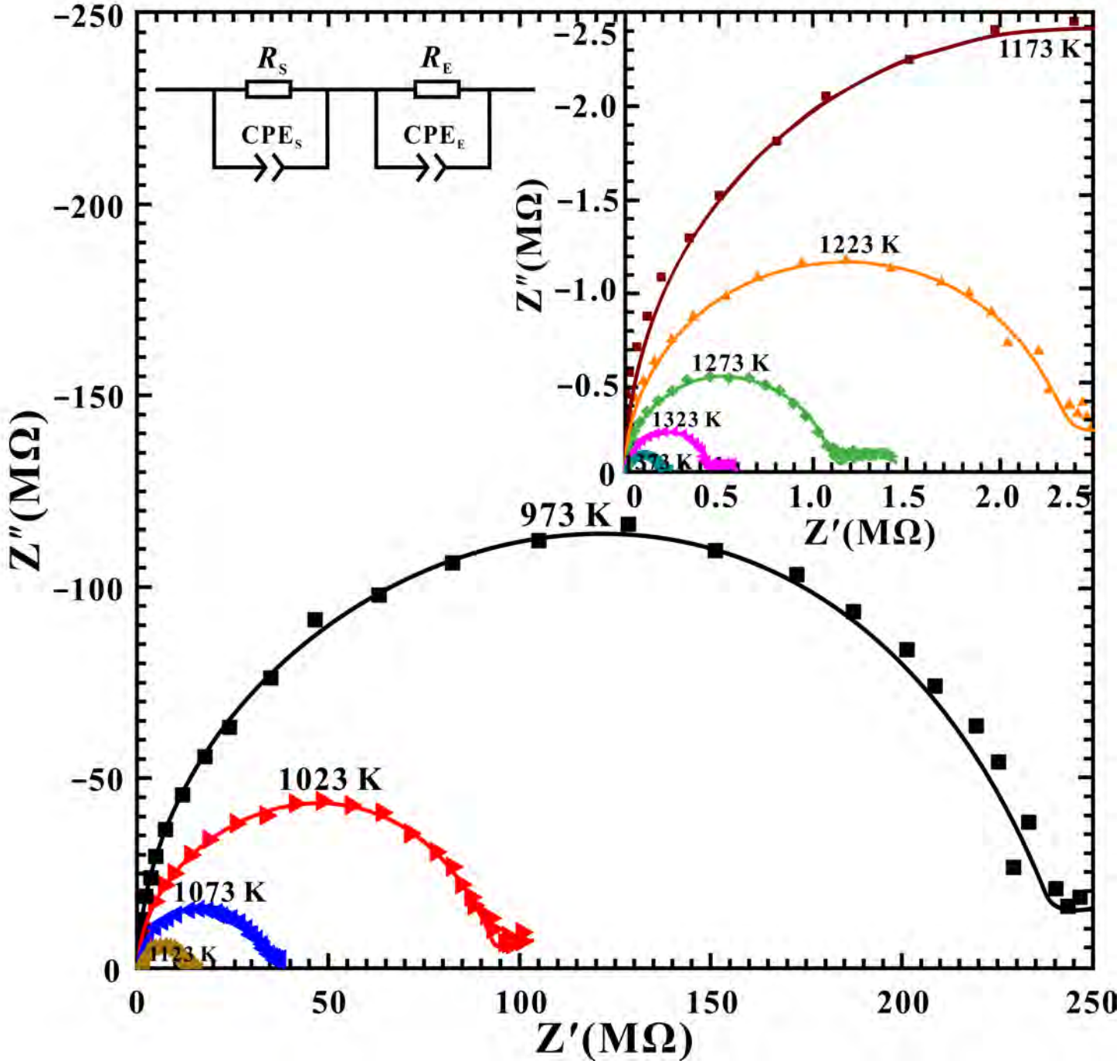

Always consult and cite the final, published document. See http:/www.minsocam.org or GeoscienceWorld

This is the peer-reviewed, final accepted version for American Mineralogist, published by the Mineralogical Society of America.
The published version is subject to change. Cite as Authors (Year) Title. American Mineralogist, in press.
DOI: https://doi.org/10.2138/am-2022-8900. http://www.minsocam.org/

Figure 5.

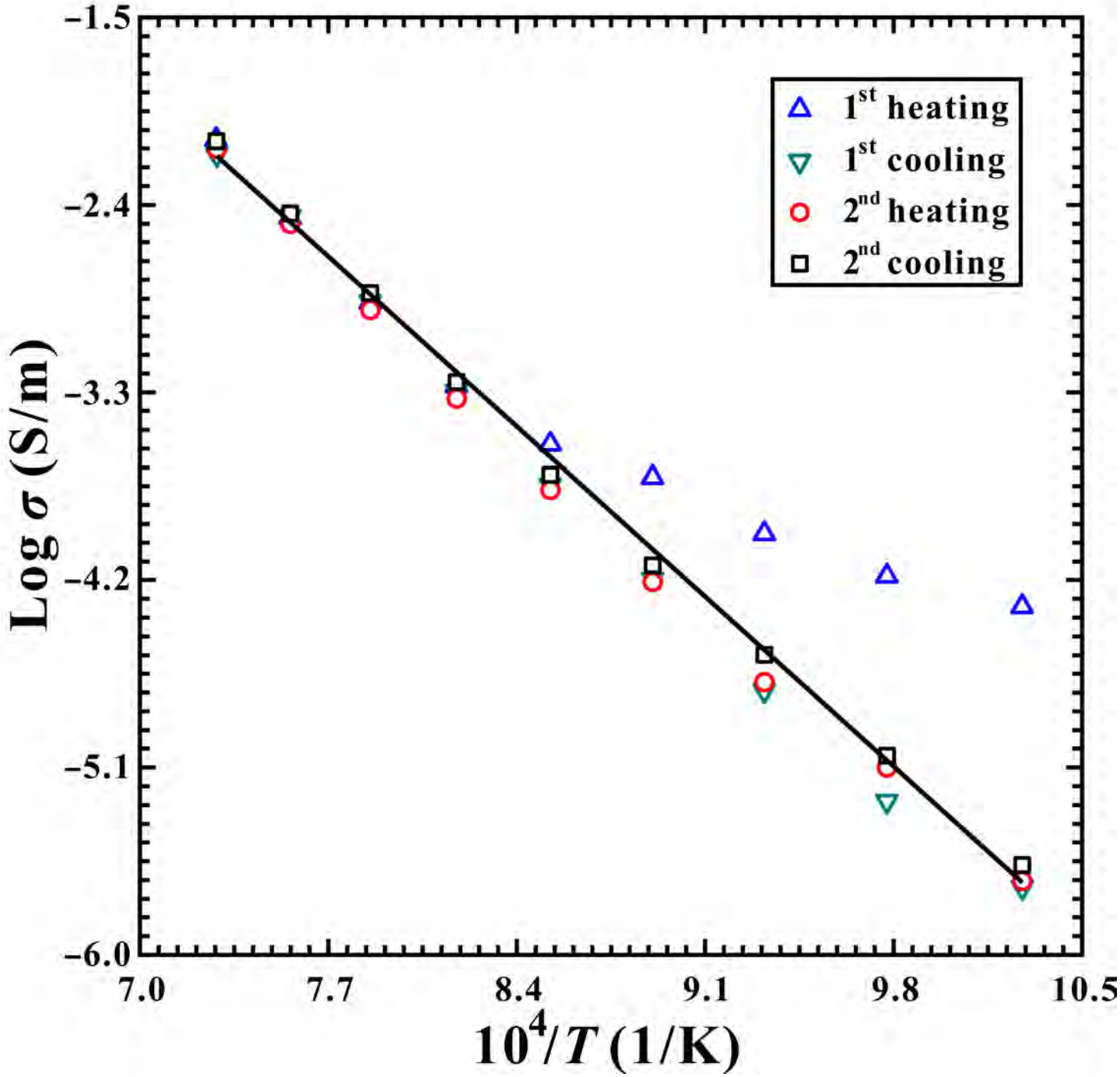

Always consult and cite the final, published document. See http:/www.minsocam.org or GeoscienceWorld

This is the peer-reviewed, final accepted version for American Mineralogist, published by the Mineralogical Society of America.
The published version is subject to change. Cite as Authors (Year) Title. American Mineralogist, in press.
DOI: https://doi.org/10.2138/am-2022-8900. http://www.minsocam.org/

Figure 6.

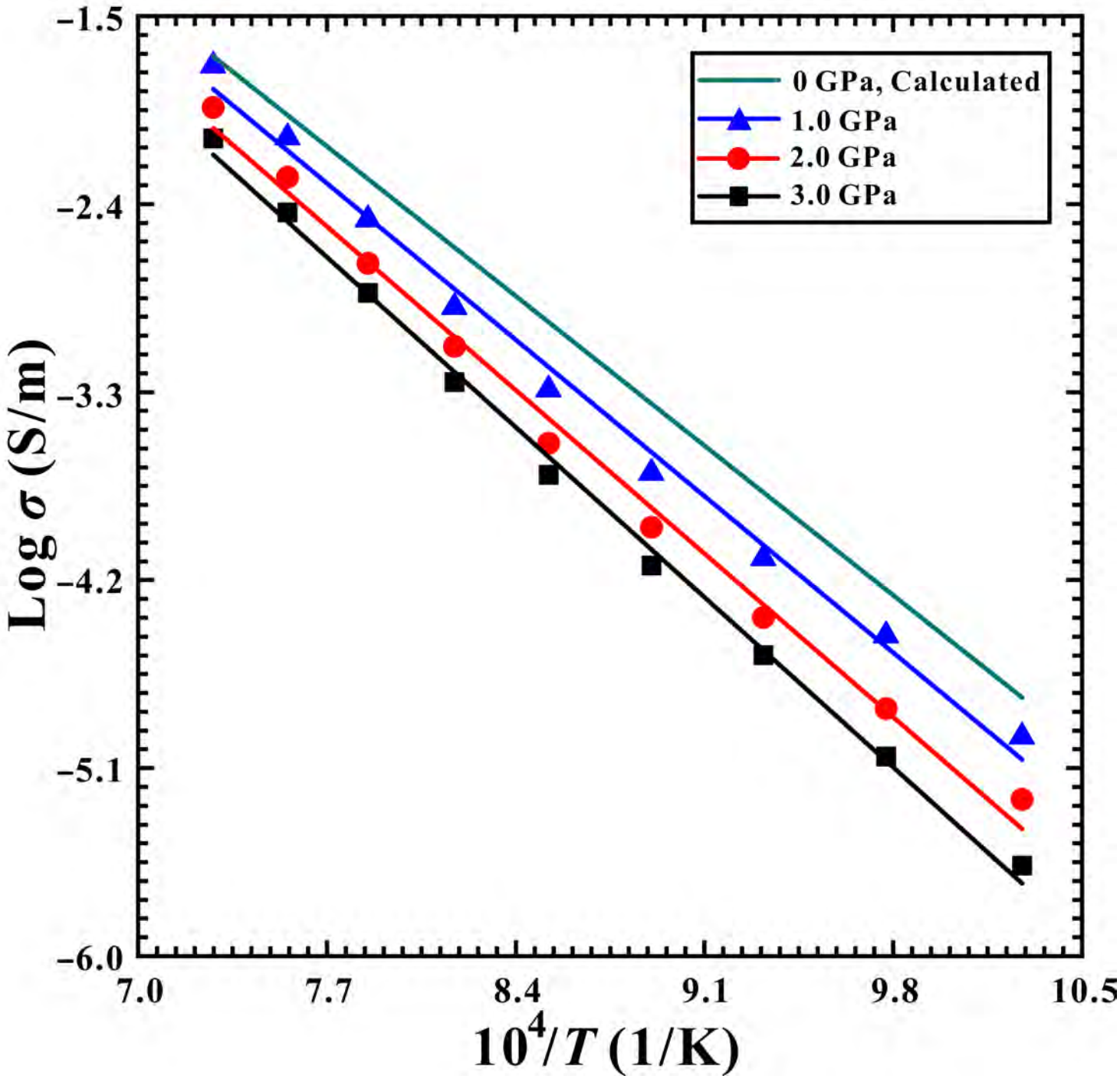

Always consult and cite the final, published document. See http:/www.minsocam.org or GeoscienceWorld

This is the peer-reviewed, final accepted version for American Mineralogist, published by the Mineralogical Society of America.
The published version is subject to change. Cite as Authors (Year) Title. American Mineralogist, in press.
DOI: https://doi.org/10.2138/am-2022-8900. http://www.minsocam.org/

Figure 7.

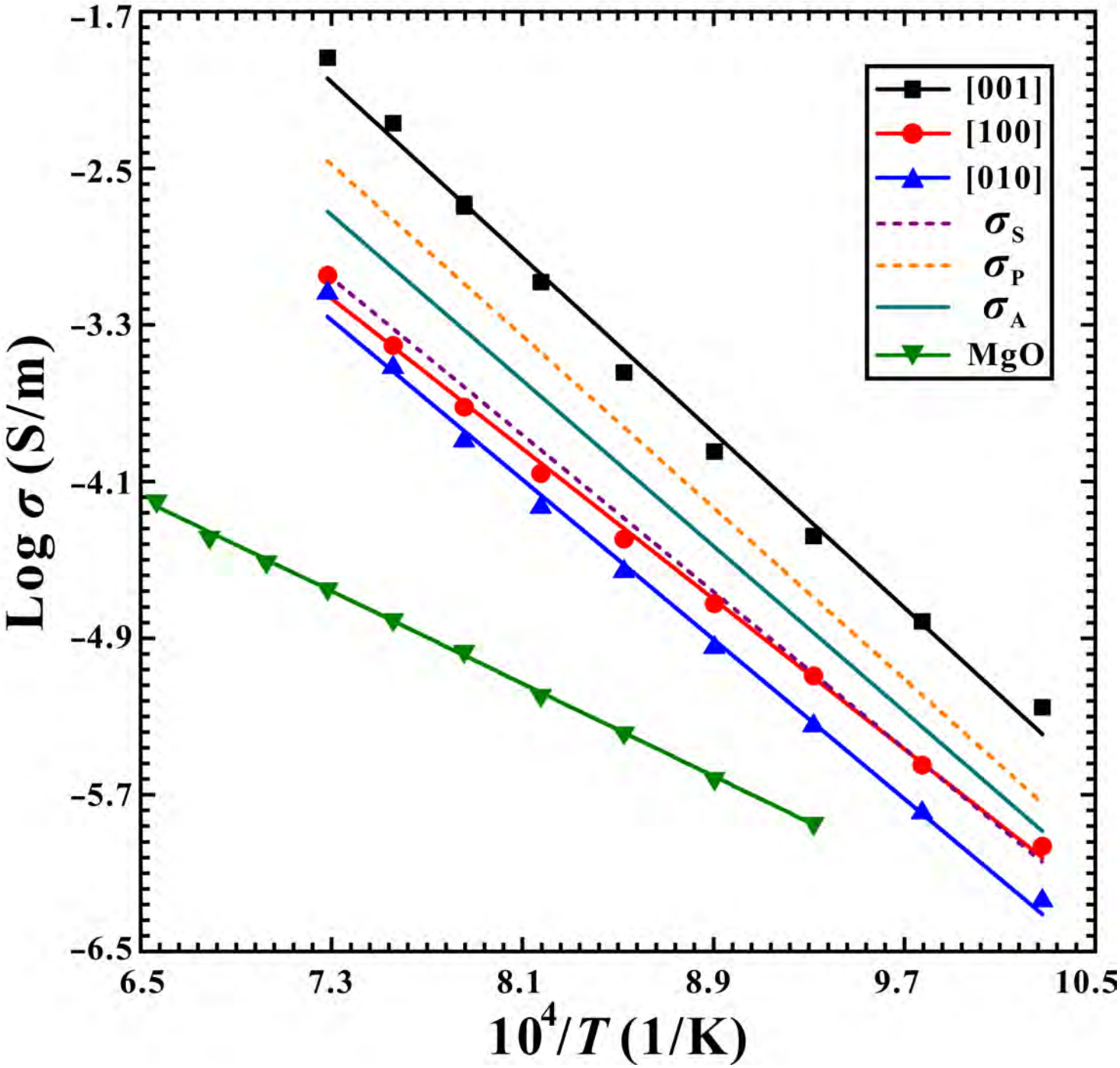

Always consult and cite the final, published document. See http:/www.minsocam.org or GeoscienceWorld

This is the peer-reviewed, final accepted version for American Mineralogist, published by the Mineralogical Society of America.
The published version is subject to change. Cite as Authors (Year) Title. American Mineralogist, in press.
DOI: https://doi.org/10.2138/am-2022-8900. http://www.minsocam.org/

Figure 8.

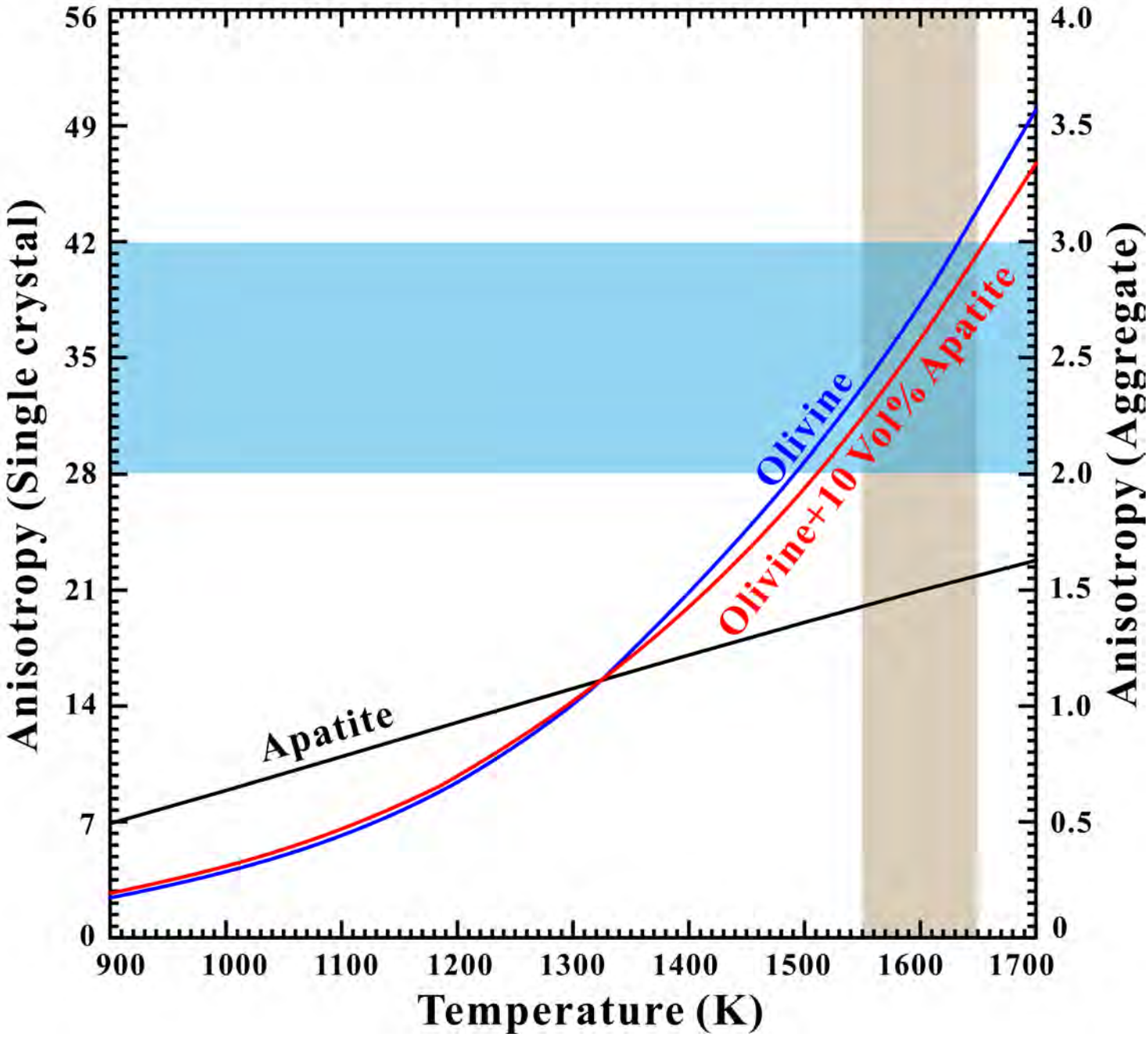

Always consult and cite the final, published document. See http:/www.minsocam.org or GeoscienceWorld

This is the peer-reviewed, final accepted version for American Mineralogist, published by the Mineralogical Society of America.
The published version is subject to change. Cite as Authors (Year) Title. American Mineralogist, in press.
DOI: https://doi.org/10.2138/am-2022-8900. http://www.minsocam.org/

Figure 9.

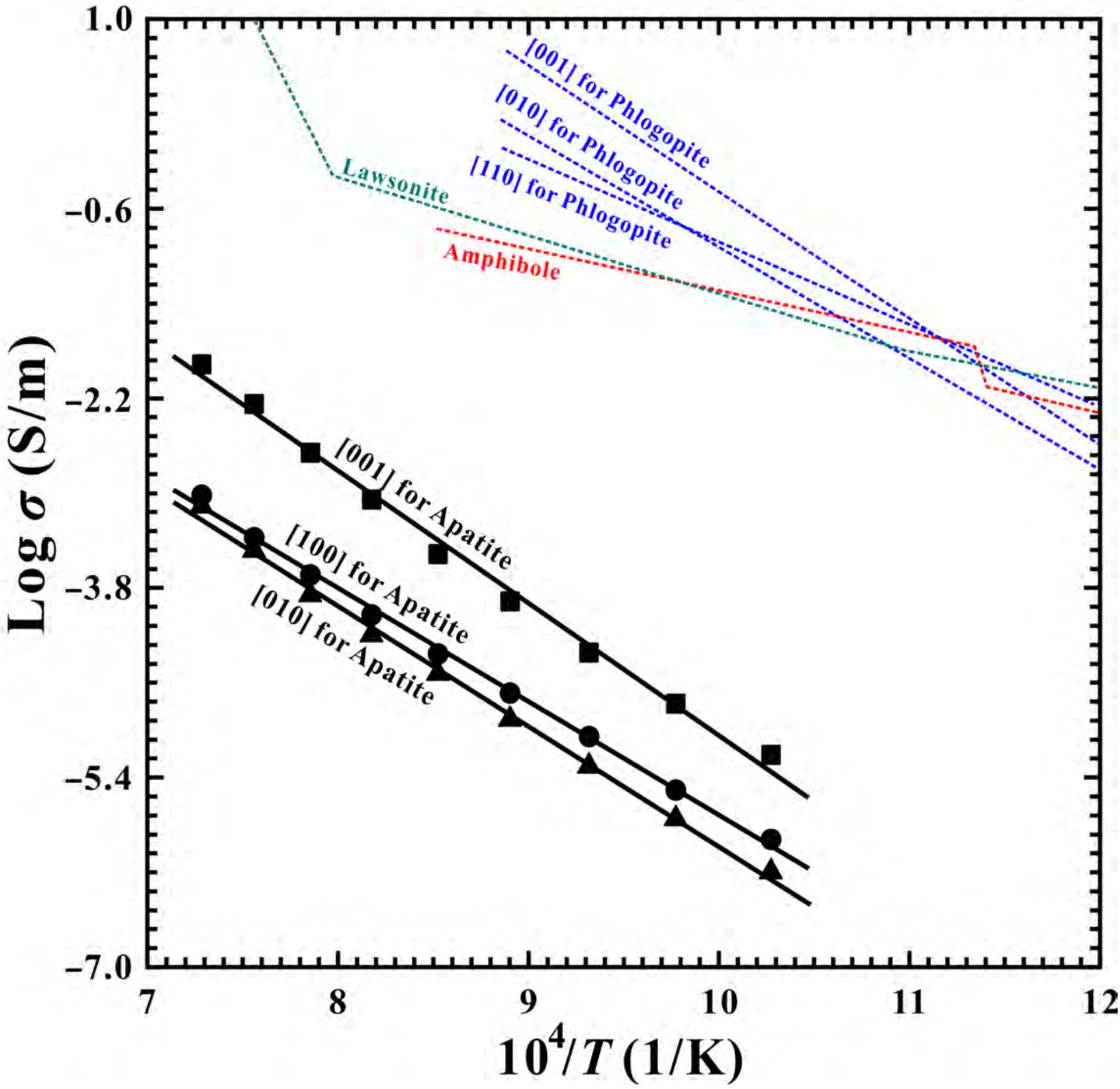

Always consult and cite the final, published document. See http:/www.minsocam.org or GeoscienceWorld

This is the peer-reviewed, final accepted version for American Mineralogist, published by the Mineralogical Society of America.
The published version is subject to change. Cite as Authors (Year) Title. American Mineralogist, in press.
DOI: https://doi.org/10.2138/am-2022-8900. http://www.minsocam.org/

Figure 10.

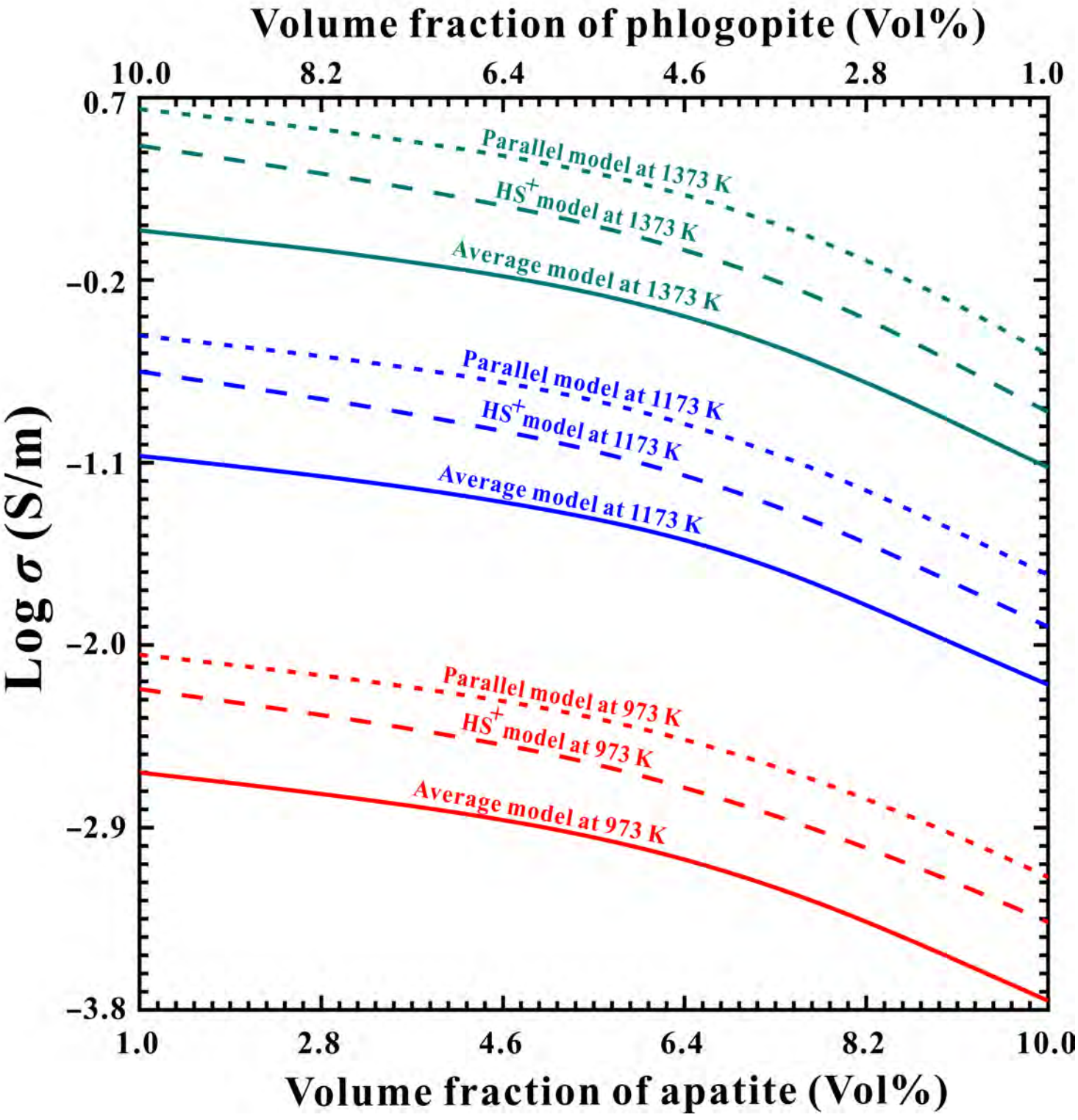

Always consult and cite the final, published document. See http:/www.minsocam.org or GeoscienceWorld

This is the peer-reviewed, final accepted version for American Mineralogist, published by the Mineralogical Society of America.
The published version is subject to change. Cite as Authors (Year) Title. American Mineralogist, in press.
DOI: https://doi.org/10.2138/am-2022-8900. http://www.minsocam.org/

Figure 11.

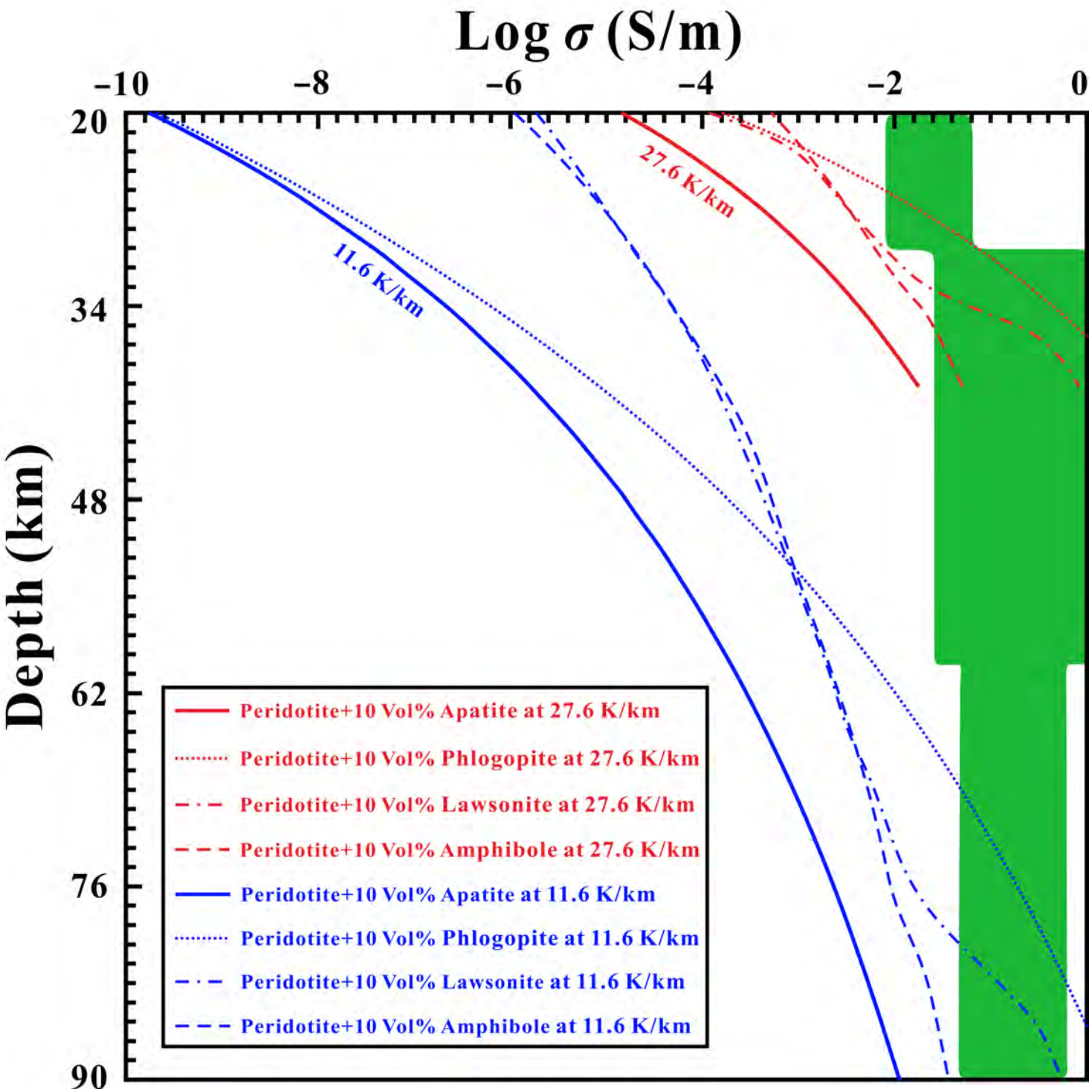

Always consult and cite the final, published document. See http:/www.minsocam.org or GeoscienceWorld